Physics – Uspekhi **59** (4) 383 – 402 (2016)

60th ANNIVERSARY OF THE JOINT INSTITUTE FOR NUCLEAR RESEARCH (*JINR*)

PACS numbers: **11.80. – m**, 13.85.Dz, 14.20.Dh

Relativistic nuclear physics at JINR: from the synchrophasotron to the NICA collider

N N Agapov, V D Kekelidze, A D Kovalenko, R Lednitsky, V A Matveev, I N Meshkov, V A Nikitin, Yu K Potrebennikov, A S Sorin, G V Trubnikov

DOI: 10.3367/UFNe.0186.201604c.0405

Contents

Abstract. We describe the development of relativistic nuclear physics at the Joint Institute for Nuclear Research (JINR) from the first experiments to our time and review the current state of the problem. The Nuclotron-based Ion Collider fAcility (NICA) at JINR and its status are described. Two goals of the project — experimental studies of dense nuclear (baryonic) matter and particle spin physics — are combined in the project based on a common experimental method: the investigation of collisions of nuclei at relativistic energies. The first problem is discussed here, and the second will be addressed in a dedicated publication. Such experiments were started at JINR in the 1970s at the Synchrophasotron proton synchrotron, and they are the main focus of the NICA project. Fundamental and applied research in other areas of science and technology that can be implemented at the NICA facility is also discussed. The accelerator facility under construction at JINR will allow performing experimental studies in particle physics at parameters and under experimental conditions that were previously inaccessible. With NICA, particle physics research in a previously inaccessible range of experimental parameters and conditions becomes possible: heavy-ion beams will be collided at center-of-mass energies in the range 4–11 GeV at luminosities up to 10^{27} cm^{-2} s^{-1}. These studies will be supplemented with experiments using a beam of extracted nuclei incident on a fixed target. A short description is given of the detectors under construction for these studies.

N N Agapov, V D Kekelidze, A D Kovalenko, R Lednitsky, V A Matveev, I N Meshkov, V A Nikitin, Yu K Potrebennikov, A S Sorin, G V Trubnikov
Joint Institute for Nuclear Research,
ul. Joliot-Curie 6, 141980 Dubna, Moscow region, Russian Federation
Tel. + 7 (496) 216 51 93. E-mail: meshkov@jinr.ru

Received 6 July 2015, revised 18 November 2015
Uspekhi Fizicheskikh Nauk **186** (4) 405 – 424 (2016)
DOI: 10.3367/UFNr.0186.201604c.0405
Translated by G Pontecorvo; edited by A M Semikhatov

Keywords: synchrophasotron, baryonic matter, mixed phase, nucleon spin, booster synchrotron, collider, luminosity, superconducting magnet, stochastic cooling, electron cooling, cryogenics

1. Introduction

1.1 Synchrophasotron: beginning of the road

Cyclotrons that accelerated particles to a maximum energy of several tens of MeVs were created in the 1930s. Because of the 'relativistic barrier', it was impossible to obtain higher energies: particle rotation and the accelerating electric field were no longer in phase. But already at that time it was clear that the development of nuclear physics required accelerators of higher energy.

In 1940, a 'cyclotron team' was established in the USSR Academy of Sciences (AS) that incorporated the 'youngsters' V I Veksler, S N Vernov, L V Groshev, P A Cherenkov, and E L Feinberg. The task assigned was to investigate the problem of constructing a cyclotron with poles several meters in diameter. Several dozen versions of the machine were considered, which only revealed the incredible complexity of the problem. However, everything changed drastically in February 1944, when Veksler cut this Gordian knot: he discovered that the relativistic barrier can be overcome by increasing the frequency of the accelerating field together with the particle energy. In this case, the phase of particle motion and that of the field automatically remain identical within a certain range of phases. This phenomenon was termed *autophasing*. The possibility arose of creating cyclic accelerators of a new class, the essential limitation of the accelerated particle energy having been overcome [1].

In the post-war hard times, the leadership of the Soviet Union made the bold decision to build an accelerator in Dubna capable of providing particles of the highest possible energy at that time — the *Synchrophasotron* (SP). Its design was prepared at the Lebedev Physical Institute (LPI) of the USSR Academy of Sciences and approved by LPI Director D V Skobel'tsyn in January 1951. The appointed project leaders were Veksler, A P Komar, M A Markov, V A Petukhov, M S Rabinovich, A A Kolomensky, and K I Blinov. The physics program was developed in 1952 by Markov, I V Chuvilo, V I Goldansky, Kolomensky, A N Gorbunov, and A E Chudakov. Within the program, problems were formulated related to the investigation of multiple particle production in proton–proton collisions, measurement of elastic and total interaction cross sections of pions and protons with protons, and searches for new particles, in particular, antiprotons; the possibility was indicated of the formation of nuclear matter composed of pions.

The proton beam obtained at the SP in March of 1957 had a record high energy of 10 GeV. The Laboratory of High Energies (LHE) led by Veksler was incorporated into the Joint Institute for Nuclear Research (JINR) and became the basis for a broad international collaboration of scientists. Commissioning of the SP gained wide attention throughout the world and was acknowledged to be an outstanding scientific achievement. The media called the machine the 'eighth wonder of the world'. Niels Bohr visited JINR in 1961 and pithily and precisely stated: "Extreme astuteness, audacity and, I would say, courage are necessary to conceive of and create such a gigantic and modern instrument."

A series of fundamental discoveries in high-energy physics was made at the SP, and development of the experimental technique led to progress in adjacent fields of science and applied research. Of the most significant physics experiments implemented in 1957–1965, the following should be noted:

— measurement of the total and differential πp-scattering cross sections [2];

— investigation of the decays of K^0 mesons; a search for antigravity effects of $\bar{K}^0$ [3];

— observation of $K_2^0 \to K_1^0$ regeneration and verification of the Pomeranchuk theorem [4, 5].

Nearly all these studies were continued successfully at the U-70 accelerator of the Institute of High Energy Physics (IHEP) and at other accelerators at higher energies.

In the same years, studies were also performed of a methodological character, which essentially enriched the options available to experiments:

— creation of an antiproton beam by the method of high-frequency separation [5, 6];

— development of gas Cherenkov counters [7];

— creation of bubble chambers and a program of studies with them [8–10];

— formation of a neutron beam and measurement of the total np interaction cross sections. Creation of a Cherenkov gamma-spectrometer and observation of the decay of vector mesons into e^+e^- pairs [11, 12];

— creation of a supersonic gas jet target [13–15].

1.2 Studies with bubble chambers

In the 1950s–1960s, 'track' bubble chambers served as important instruments for the observation of particle interactions. They exhibited a number of remarkable advantages: the possibility of filling the chambers with various liquefied gases (hydrogen, propane, xenon, and others), which served simultaneously as a dense target and as a sensitive medium owing to the large volume of particle registration (up to several cubic meters) and to the high measurement accuracy (about 200 μm) of coordinates of points along the tracks (particle trajectories), etc. During the period of 1955–1970, several gas and bubble chambers were constructed at the LHE, JINR; the largest of them was a two-meter liquid-hydrogen bubble chamber [8–10] 2 m in length along the beam, which was later supplemented with a track-sensitive deuterium target.

Below, only some of the results are listed that were obtained with bubble chambers irradiated with particles accelerated at the SP to an energy of 3–10 GeV and, subsequently, at the U-70 accelerator with 70 GeV protons and 40 GeV pions:

• 'baryon charge inertia' was revealed: the angular distribution of baryons in pp and πp interaction events was distinctly anisotropic in the center-of-mass system (CMS). In pp interactions, baryons form two cones directed forward and backward along the axis of the particle beam incident on the target. These particles are termed leading because their momenta significantly exceed the mean value of particle momenta in a given event. In πp collision events, baryons only form a single backward cone. The concept of a *target and beam fragmentation region* was introduced for the forward–backward cones. The remaining portion of events was said to belong to the *pionization region*. It was later also called the *central region*;

• the momentum correlations of identical and nonidentical particles were measured. The space–time size of the interaction region was determined. Application of the technique, first developed at the LHE and subsequently called *femtometry*, has now become widespread. It permits characterizing different models of multiple particle production;

• extensive data were obtained concerning nucleus–nucleus interactions: dC, CC, CTa, and interactions of antiprotons, antineutrons, and antideuterons with protons, deuterons, and other nuclei. These data are still relevant and serve for developing theoretical models of collisions of nuclei and antinuclei (Fig. 1);

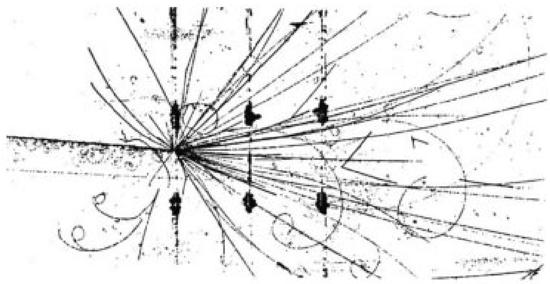

Figure 1. Typical collision event of a carbon (C) nucleus of the energy 4.5 GeV/nucleon with a tantalum (Ta) nucleus. The photograph was made in a propane chamber 2 m long along the beam axis with Ta plates as a target.

• in 1960, the first event was observed of the production of the $\overline{\Sigma}^-$ antihyperon. This discovery was also made with a propane chamber. It is interesting to note that four strange particles were also observed, which was the first experimental evidence of multiple strange particle production [16];

• an unexpected spin alignment was discovered for ρ^0 mesons produced in antiproton–proton interactions, and its relation to the polarization of valence quarks in the course of their fusion was revealed [17].

1.3 Investigation of diffraction processes in hadron collisions

In the 1960s, a very exciting and widely discussed issue was the asymptotic behavior of hadron interactions: how do the total cross sections and amplitudes of binary processes behave with an unlimited increase in particle energy? The simplest and therefore most attractive assumption was based on the so-called optical model, according to which the total cross sections $\sigma_{\text{tot}} = 2\pi r^2$ and the slope of the diffraction cone $\mathrm{d}\sigma_{\text{elast}}/\mathrm{d}t \approx \exp(bt)$, where $b = r^2/2$, $t < 0$ is the squared 4-momentum, transferred to the scattered particle, tend to constant values as $E \to \infty$, because a hadron, being an extended object, is an absorbing (grey or black) sphere of a constant radius r significantly exceeding its de Broglie wavelength λ: $r \gg \lambda = h/p$. Accordingly, the real part of the elastic scattering amplitude A, which in optics is due to not diffraction but the refractive index, tends to zero: $\rho(E) = \operatorname{Re} A/\operatorname{Im} A \to 0$. If the parameter $\rho(E)$ is known, it is possible to verify the dispersion relations that relate the real and imaginary parts of the elastic scattering amplitude of particles. The dispersion relations are derived from basic postulates of quantum field theory: causality, unitarity, Lorentz invariance, and spectrality.

In the early 1960s, the concept *of Regge poles* was formulated, and it was claimed it would become the main element of the strong interaction theory. According to 'Reggistics', the leading contribution to binary processes and total cross sections at a sufficiently high energy is made by a single pole, the *pomeron*:

$$\frac{\mathrm{d}\sigma(s,t)}{\mathrm{d}t} = f(t)\left(\frac{s}{s_0}\right)^{2\alpha(t)-2}, \qquad \alpha(t) = \alpha(0) + \alpha' t,$$
$$\sigma_{\text{tot}}(s) = \sigma_0 + \sigma_1\left(\frac{s}{s_0}\right)^{\alpha(0)-1}, \qquad b(s) = b_0 + 2\alpha' \ln\frac{s}{s_0}, \tag{1}$$

where $\mathrm{d}\sigma/\mathrm{d}t$ is the differential elastic scattering cross section of the particles being studied, σ_1 and σ_0 are parameters determined by the experimental data, $f(t)$ is an arbitrary function depending on the experimental data, s is the squared CMS energy of a pair of interacting particles, and s_0 is a normalizing constant (usually assumed to be $s_0 = 1\ \text{GeV}^2$). The function $\alpha(t)$ is called the pomeron trajectory. Parameters $\alpha(0)$ and α' determine the type of asymptotic behavior. When $\alpha(0) < 1$, we have an asymptotic form with decreasing or constant total cross sections; at $\alpha(0) > 1$, the cross sections increase polynomially. If $\alpha' = 0$, we have an analog of classical optics with $b = \text{const}$. If $\alpha' > 0$, then the parameter b (and the radius of the interaction region) undergo a universal logarithmic increase in all diffraction processes.

Thus, experiments were confronted with the problem of verifying relations (1). Estimates showed the necessity of performing measurements with a high precision ($\sim 2\%$ in the case of differential cross sections) and within a broad range of energies $E > 5$ GeV.

Studies of pion and proton elastic scattering on protons and light nuclei started at JINR literally simultaneously with the first laps of the SP beam. In the early 1960s, groups led by V A Sviridov and L N Strunov proposed two new techniques that turned out to be quite effective. To observe scattering of pions, a Wilson cloud chamber filled with gaseous hydrogen was used. The novelty of the experiment lay in the application of a special operation mode of the chamber with reduced sensitivity in the case of a high beam intensity. The slow and strongly ionizing recoil protons from elastic scattering were then registered in the gas with high efficiency. The new operation mode permitted registering elastic scattering events with a record small momentum transfer and obtaining large statistics. Moreover, a thin film target (about 0.5 μm thick) was installed in the internal SP beam, permitting the accelerated particle beam to cross the target repeatedly. In 1967, this experience was used in creating the target in the internal beam of the U-70 accelerator. The target also had an essentially new element, a gaseous supersonic hydrogen jet [18–21].

The method involving a thin internal target has at least three important features:

— the possibility of accelerating particles within the whole range of accelerator energies (scanning) and having other experiments performed at the same time;

— the possibility of precision measurements of the energy and emission angle of a slow recoil particle;

— no need in an extracted beam, which significantly reduces the cost of the installation and permits physics measurements to be initiated immediately upon commissioning the accelerator.

With the aid of the thin-internal-target method, studies of elastic proton scattering on protons and deuterons were performed at the SP [18–21].

By the middle of 1969, the discussion of the asymptotic behavior type in hadronic processes had still not led to any clarity. The elastic pp-scattering data obtained at JINR in the 2–10 GeV energy range (Fig. 2) pointed to a narrowing of the

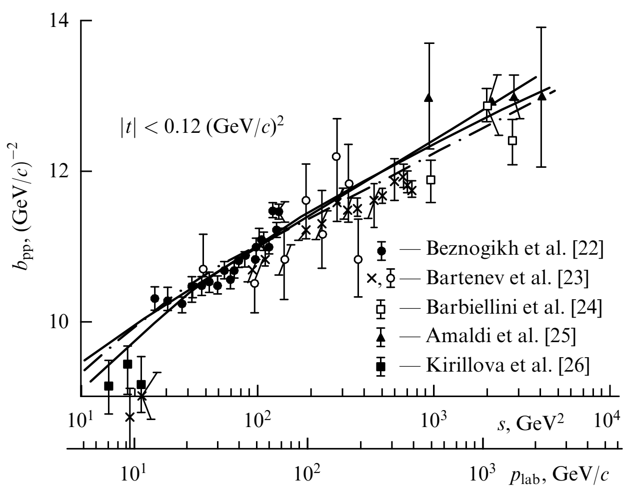

Figure 2. Compilation of the most precise data (in 1973) on the slope parameter $b_{\text{pp}}(E)$; t is the squared four-momentum transfer in the elastic scattering process of a pair of particles, s is the squared CMS energy of the particle pair, and p_{lab} is the incident particle (proton) momentum in the laboratory system.

diffraction cone. The data obtained by the Brookhaven National Laboratory and by CERN in the 15–24 GeV energy range pointed to the leveling of the functions $\sigma_{\rm tot}(E)$ and $b(E)$. However, the low measurement accuracy did not permit any convincing conclusion to be drawn. The original research method and the broad energy range achieved at the U-70 accelerator, the largest in 1968–1972, permitted the raised question to be answered. The first announcement of the results obtained at U-70 for the parameter b was made in the summer of 1969 at the Lund conference [22]. The experiment unambiguously revealed a logarithmic increase in the function $b(E)$. The trajectory slope of the effective Pomeranchuk pole [α' in formula (1)] turned out to differ from zero: $\alpha' = 0.47 \pm 0.09$. The expression 'effective pole' reflects the approximate character of formulas (1). Attempts at the formulation of a more precise and complete concept of Regge poles are still under way. The project TOTEM (TOTal Elastic and diffractive cross-section Measurement) at the LHC at CERN is devoted to this problem.

Studies performed at the SP and U-70 in the late 1960s upon the commissioning of these accelerators played an important part in shaping the concept of a pomeron and in determining its properties. At present, this object continues to play an important role in describing the dynamics of soft and semihard hadron processes, including inelastic diffraction. The pomeron has acquired the status of a nearly real hadron. In experimental studies of deep inelastic lepton scattering, attempts are made to determine its structural function in terms of quarks and gluons.

1.4 Discovery of the decays of vector mesons into e^+e^- pairs

In the 1960s, much attention was paid to experimental and theoretical investigations of the leptonic decay of vector mesons. This process is very important for testing the SU(3) symmetry of strong interactions, the $\omega^0 - \varphi^0$ mixing hypothesis, and the vector dominance (VD) model. The phenomenological VD model was proposed to describe the interaction of a photon with hadrons (Fig. 3). The model was based on the assumption that a photon interacting with hadrons transforms first into vector mesons ρ^0, ω, φ, and then into their excited states. Thus, a photon (light!) exhibits hadronic properties. The photon and vector mesons have the same quantum numbers. Therefore, transformation of a photon into a vector meson is not forbidden, unlike transitions into other mesons. The VD model is widely used within the energy range of the order of several GeV. This is because accurate calculations based on quantum chromodynamics in the relevant energy range are extremely complicated. But predictions of the VD model are in good agreement with experimental results.

The resonance character of the production process of K^+ and K^- mesons in the e^+e^- annihilation reaction is well described by a diagram in which the photon first transforms into a φ meson and the latter then decays into a pair of K^+ and K^- mesons. The energy of the resonance in this process coincides with the rest energy of the φ meson.

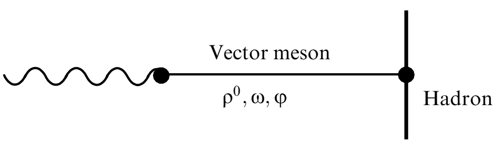

Figure 3. Interaction of a photon with a hadron. The photon transforms into a vector meson that interacts with the hadron.

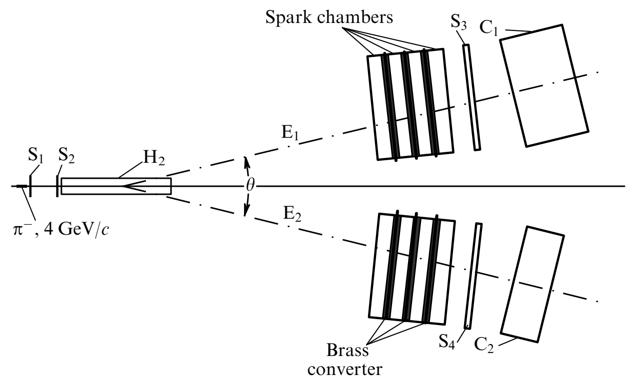

Figure 4. Layout of the installation for observing the production reaction and lepton decay of vector mesons. $S_1 - S_4$ — scintillation trigger detectors; H_2 — liquid-hydrogen target 50 cm long; C_1 and C_2 — total absorption Cherenkov γ-spectrometers.

Other evidence in favor of the VD model is as follows: the interaction cross section of a photon with a nucleus composed of A nucleons must be proportional to the mass number A. From experiments, however, it follows that the cross section behaves as $\sigma = \alpha A + \beta A^{2/3}$. The second summand is due to the photon, which has transformed into a vector meson before interacting with the nucleus. Thus, some of the nucleons turn out to be screened as a result of the strong interaction of a virtual meson with the nucleus.

Observation of the production and leptonic decay of vector mesons $V \equiv (\rho^0, \omega^0, \varphi^0)$,

$$\pi^- + p \to V + n \to e^+ + e^- + n\,, \qquad (2)$$

was first achieved at the JINR SP [27] in a beam of π^- mesons with momenta of 4 GeV/c. The installation, whose layout is shown in Fig. 4, is a two-arm Cherenkov total absorption spectrometer. An important feature of this spectrometer is the presence of spark chambers, which measure the coordinates of charged particles with an accuracy of ≈ 2 mm. Each arm of the spectrometer contains 90 counters, which are radiators made of optical lead glass. The length of a counter is 35 cm, which amounts to 14 radiation lengths; the shape of its transverse cross section is a hexagon 17.5 cm in size. The energy resolution of the counter is $\approx 5\%$. The registered effective mass range of an e^+e^- pair 500–1200 MeV, and the mass resolution is 40 MeV. Thirty-eight events of reaction (2) have been registered. The result obtained is

$$B_\rho \sigma_\rho + B_\omega \sigma_\omega = (0.5 \pm 0.1) \times 10^{-4}\ \text{mb}\,,$$
$$B_\varphi \sigma_\varphi = (0.17 \pm 0.1) \times 10^{-4}\ \text{mb}\,,$$

where $B_V = \Gamma(V \to e^+e^-)/\Gamma(V \to \text{total})$ is the ratio of vector meson decay widths, and σ_V is the total V-meson production cross section in reaction (2). The smallness of the cross sections manifests the extreme complexity of the work fulfilled. The relative leptonic decay widths are also presented:

$$B_\rho = (5.3 \pm 1.1) \times 10^{-5}\,, \qquad B_\omega = (6.5 \pm 1.3) \times 10^{-5}\,.$$

The results obtained contributed to the development and improvement of the aforementioned theoretical concepts.

Later measurements enhanced the precision of the SP data but changed the actual values insignificantly.

1.5 Formation of charged particle beams with the aid of a bent crystal

The possibility of bending a beam of charged particles by channeling into a bent crystal was shown theoretically by Tsyganov [28] in 1976, and shortly after this amazing effect was demonstrated with the extracted SP proton beam [29]. The phenomenon of particle channeling in a crystal, which had been known previously, consists in the motion of a charged particle under the influence of an electric field of ions localized between planes of the crystal lattice. If the angle between the trajectory and a plane is sufficiently small, the particle is reflected from the plane, and its motion takes place between such planes. Channeling in a mechanically bent crystal results in bending of the particle beam.

In the very first experiment at the SP, an 8.5 GeV proton beam was bent an angle of 26 mrad by a silicon crystal about 5 mm long. The crystal turned out to be equivalent in bending capacity to a magnet of the same length exhibiting a field strength of 60 T!

The pioneering work performed at the SP opened a new road for experimental techniques: beam extraction from the accelerator, the formation of secondary particle beams, the construction of essentially new focusing elements, and the measurement of beam emittance and of the magnetic moments of short-lived particles [30]. First implemented at the SP, this technique was also confirmed at the Super Proton Synchrotron of CERN and at the Tevatron of the Fermi National laboratory (USA). At the IHEP U-70 accelerator, bent crystals were used to prepare several extracted proton beams with energies up to 70 GeV [31].

1.6 Investigation of cumulative processes

An analysis of experimental data on the interaction of leptons, protons, and nuclei with protons and nuclei obtained in the early 1970s led to the idea of *scale invariance* of inelastic processes. This term signifies a similarity between secondary hadron spectra at different energy values of the primary particles. This property of the spectra is also called *self-similarity* or *scaling*. Data analysis has shown that to represent the cross section of an inclusive process $A + B \to C + X$ (the sole particle C being observed), it is convenient to introduce the dimensionless scale variable $x = p_C/p_{C\max}$, where the denominator is the kinematically largest possible momentum of particle C, which is assigned the role of a scale parameter. Then the cross section $\mathrm{d}\sigma/\mathrm{d}p_C(s, p_C) = f(x)$ turns out to be a universal function $f(x)$ that does not depend on energy.

In 1971, Baldin [32, 33] put forward the following hypothesis: in the case of relativistic hadrons, cross sections such as $f(x)$ depend only on the local properties of hadron matter, but not on the geometric characteristics of the interacting objects A and B (for example, the form factors). As a result, the problem of providing a relativistic description of excited hadron matter and of extended composite objects arose. Thus, the age of *relativistic nuclear physics* came into being.

One of the striking phenomena among these problems is the *cumulative effect*, discovered experimentally in the d + Cu reaction, where the production was observed of π mesons with momenta significantly exceeding the values following from the energy–momentum conservation in pair collisions of nucleons belonging to the deuteron and the carbon nucleus. A possible description of cumulative processes in the collision of two nuclei (A, B) could be based on the excitation mechanism of a group of N^* nucleons, $N_{AB} \to N + N^*$. The number of nucleons N^* depends on the mass of the nucleus (A or B), and the probability $P_N(N)$ of the association of N^* nucleons has to be determined by simulation, for instance, by calculations considering it to be consistent with a binomial law. Then the general form of the cross section is expressed as

$$E\,\frac{\mathrm{d}\sigma}{\mathrm{d}p} = \sum_{N_{\min}}^{A} P_N(N) f_N(x_N)\,. \tag{3}$$

The minimal number of nucleons in the association is determined by the kinematic relation (in units such that $c = 1$) $N_{\min} = (E^* - P^* \cos\theta^*)/m \approx Q$, where θ^* is the angle between the vector momenta of N particles and N^* nucleons. The value of $N_{\min}$, denoted by Q, is called the *cumulative number*.

The first experimental test of the cumulative effect hypothesis was carried out in 1971 by the group of Stavinsky in beams of protons and deuterons accelerated at the SP to a momentum of 10 GeV/c [34]. The momentum of a single nucleon in the deuteron was about 5 GeV/c. Measurements were performed of the cross sections of the inclusive reactions $\mathrm{p} + \mathrm{Cu} \to \pi^- + X$ and $\mathrm{d} + \mathrm{Cu} \to \pi^- + X$. The spectrum of pion momenta in the second reaction turned out to be extended significantly higher than the boundary imposed by the energy–momentum conservation law for a pair of interacting nucleons. Analysis of the data by formula (3), where the function P_2 is calculated in the momentum approximation, yielded a calculated spectrum of cumulative pions 2–4 orders of magnitude lower than the experimental spectrum. Thus, the existence was demonstrated of the cumulative effect, as well as of its consistency with scale invariance and with the quite simple model for the joint action of two nucleons.

A measurement of the emission of protons at an angle of 137° from a fragmenting carbon nucleus in a p + C reaction at an incident proton energy of 1–6 GeV is presented in Ref. [35] (Fig. 5). The arrows in the figure indicate the momenta that a proton scattered quasielastically on

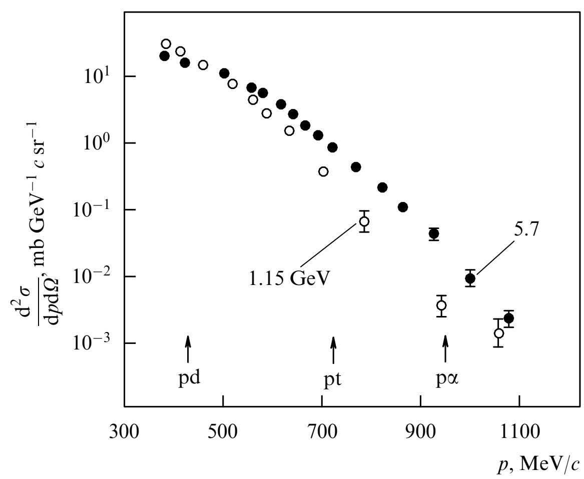

Figure 5. Proton spectrum in the reaction $\mathrm{p} + \mathrm{C} \to \mathrm{p} + X$ at the beam proton energies 1.15 and 5.7 GeV. The secondary proton is registered at an angle of 137°. The arrows show the positions of quasielastic maxima expected in the case of proton scattering on clusters d, t, α.

nucleonic clusters d, t, α could have in accordance with the kinematics. The cumulative region $p_{\rm p} \geqslant 400$ MeV$/c$ is clearly seen. However, no peculiarities (peaks) are seen in the spectrum. Once again, this demonstrates the 'parton' character of the processes investigated: instead of individual nucleons, *partons* (groups of particles), carrying a significant part of the momentum of a group of several nucleons, take part in the interaction. Thus, collisions of nuclei reveal more complex dynamics of particle production than in the case of nucleon–nucleon pair collisions.

The beginning of experiments in the field of relativistic nuclear physics stimulated numerous investigations of the properties of highly excited nuclear matter, aimed at studying the color degrees of freedom in nuclei and quantum chromodynamics (QCD) at long distances. The discovery of cumulative pions initiated the study of color degrees of freedom in collisions of relativistic nuclei. Furthermore, detailed investigations of cumulative production processes required an enhanced intensity of proton and deuteron beams at the SP and led to the establishment of the boundaries of the limit fragmentation domain. This boundary corresponds to the value $\sqrt{s_{NN}} \approx 3.2$ GeV.

Further experiments with p, d, π, γ, ν beams with targets from deuterium to uranium involving the registration of cumulative pions, kaons, protons, antiprotons, deuterium, tritium, and helium nuclei in the energy range of interacting particles from 1 to 400 GeV at the accelerators of the LHE, JINR and also at the Institute of Theoretical and Experimental Physics (ITEP, Moscow), at IHEP (Protvino), at the Yerevan Physics Institute, and at the Lawrence Berkeley National Laboratory (LBL) (USA) confirmed the results presented in Refs [34, 35]. These results served as serious justification for the development of the JINR accelerator base, which led to the creation of the first superconducting relativistic proton synchrotron in our country, the Nuclotron (1987–1992), constructed under the guidance of Baldin [32, 36].

In those same years, beams of polarized deuterons accelerated in the SP to 4.5 GeV per nucleon were used to perform experiments aimed at studying the spin physics of a nucleon, which were subsequently continued at the Nuclotron.

The success of the Standard Model, confirmed by precision experiments at colliders at the end of the 20th and beginning of the 21st centuries, led to the formation of a firm opinion that 'new physics' in the baryon sector can only be found at *superhigh energies*. The discovery of the Higgs boson at the LHC seemed only to strengthen this attitude (the Future Circular Collider project at CERN), according to which nothing significant is to be expected within the range of CMS hadron energies between 10 and 20 GeV. However, it turns out, as we have demonstrated above with the example of the cumulative effect, that this is far from true.

1.7 Revelation of expansion of the pion production volume in *NN*- and *AA*-interactions

A *Hybrid magnetic spectrometer* (HYBS) [37] has been constructed on the extracted SP beam for investigating the interactions of nuclei and protons. The main element of the setup is a streamer chamber with a fiducial volume of $188 \times 77 \times 58$ cm^3 placed in an electromagnet. The target can be either outside or inside the chamber. The spectrometer provides registration of the interaction products of the beam with the target within the full solid angle (4π geometry). A set of trigger counters permits selecting rare or high-multiplicity events with a high time resolution. Below, the results of one such study are presented.

An important line of research in the field of relativistic nuclear physics at accelerators in operation and under construction is based on the possibility of obtaining an answer to the question concerning the collective dynamics of a system composed of a large number of particles. Clearly, for new states of nuclear matter to form, the best objects are nucleus–nucleus interactions involving a maximum number of participating nucleons, i.e., events of central nuclear collisions. To identify such events, at least two criteria are applied: a large multiplicity of secondary particles and a minimal flux of particles within a certain small angular cone with respect to the beam axis.

Paper [38] is devoted to the investigation of multiple particle production in central collisions of magnesium nuclei at an energy of 4.3 GeV per nucleon and in neutron–proton collisions at 3.8–5.2 GeV$/c$ using the extracted SP beam. Mg + Mg interactions are registered in the HYBS streamer chamber, while n + p interactions are registered in a liquid-hydrogen bubble chamber at the LHE. To identify central Mg + Mg collisions, the HYBS setup is equipped with a set of trigger counters that note a high multiplicity within a broad interval of angles and a minimal particle flux at a small angle close to 2.4°. π^--meson pairs are analyzed. The experimental material includes 470,000 pairs in central Mg + Mg collisions and 45,000 pairs in n + p events. These data are used to construct the correlation function

$$C(q) = \frac{\mathrm{d}^4\sigma/\mathrm{d}q^4}{(\mathrm{d}^4\sigma/\mathrm{d}q^4)_{\rm backg}}\,.$$

where $q = (q_0, \mathbf{q}) = p_1 - p_2$ is the 4-momentum difference for the pion pair. The denominator is the background distribution obtained by random selection of each particle in the pair. The correlation function can be written for an element of the excited nuclear system that moves relative to the observer with a speed β [39]:

$$C(q) = 1 + \lambda\left[-\gamma^2(q_\parallel - \beta q_0)^2 R_\parallel^2 - q_\perp^2 R_\perp^2 - \gamma^2(q_0 - \beta q_\parallel)^2 T^2\right]. \tag{4}$$

Here, $R_\parallel$, $R_\perp$, and T are the space and time dimensions of the selected system element in its own reference frame, while the momenta q are measured in the reference frame of the observer. Formula (4) takes the interference of identical pions into account. An element is understood to be a sample of pions from a certain volume of the momentum space.

In Ref. [38], the entire system is divided into six elements (cells). The data of each element are described by formula (4) by the method of least squares or by the maximum likelihood method, and the parameters λ, β, $R_\parallel$, $R_\perp$, and T are found. The range of $|q|$ is 10–200 MeV$/c$. The pion momentum and angle measurement accuracies are about 1% and 5 mrad. The following parameters were obtained for the Mg + Mg system:

$$R_\parallel \approx (4.5 \pm 0.5)\ \text{fm}\,, \qquad R_\perp \approx (3.0 \pm 0.3)\ \text{fm}\,,$$

$$T \approx (3.0 \pm 1.5)\ \text{fm s}^{-1}\,, \qquad \lambda \approx 0.8 \pm 0.1\,.$$

The parameters of the n + p system are

$$R_\parallel \approx R_\perp \approx (1.6 \pm 0.3)\ \text{fm}\,, \qquad T \approx (1.5 \pm 0.3)\ \text{fm s}^{-1}\,.$$

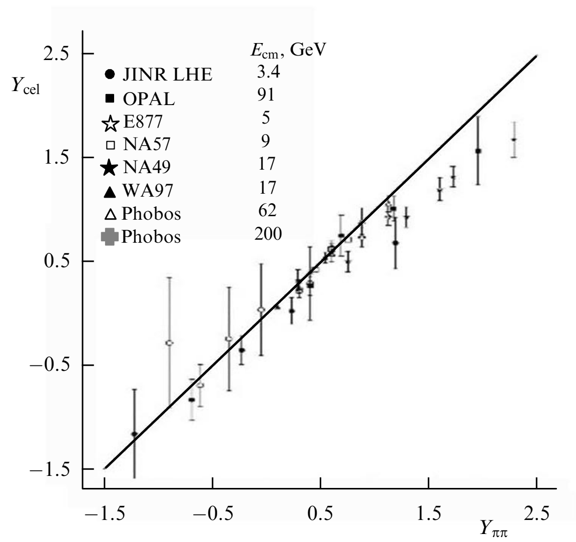

Figure 6. Compilation of data on the dependence of the pion generation cell rapidity Y_{cel} on the average rapidity of a pion pair $Y_{\pi\pi}$. Presented are the results obtained at the LHE with the aid of SKM-200 and 'Hydrogen bubble chamber' facilities, as well as data from later experiments confirming the LHE results.

These values depend weakly on the choice of the rapidity (momentum) interval of the element.

We now make the rapidity of a given element (cell) correspond to the parameter β: $Y_{cel} = (1/2)\ln[(1+\beta)/(1-\beta)]$. We determine the mean rapidity of the pion pair in the cell, $Y_{\pi\pi} = \langle Y_{\pi 1} + Y_{\pi 2}\rangle/2$. Figure 6 presents the dependence $Y_{cel}(Y_{\pi\pi})$. The quantities Y_{cel} and $Y_{\pi\pi}$ turn out to be strictly correlated: $Y_{cel} \sim Y_{\pi\pi}$ is the straight line in Fig. 6. This is a clear proof of expansion of the pion generation volume.

The following results are obtained and presented in Ref. [38]:

— a new experimentally measurable parameter of interference analysis — the speed of an element of the pion generation volume — has been introduced for the first time. The speeds of such elements have been measured and turned out to be close to the average speeds of the respective pion ensembles;

— expansion of the pion generation volume has been observed for the first time in the longitudinal and transverse directions. The character of expansion is the same in Mg + Mg and n + p interactions;

— the space–time dimensions of pion generation elements have been measured for the first time in their own reference frame. The incorrectness of the determination of dimensions of a frame moving with respect to the observer has been noted.

1.8 Fragmentation and phase transitions in hot nuclei

The liquid drop model of a nucleus developed in the 1930s is successfully applied to analyze the interaction of nuclei at a low excitation energy (temperature T) $E_N = T \leqslant T_c$. Here, E_N is the average energy of a nucleon in a nucleus and $T_c \approx 15$ MeV is the critical temperature, which cannot exceed the nucleon binding energy. In the region $T \leqslant T_c$, the nucleus is metastable. It reduces its energy by evaporating particles. In the region $T > T_c$, the nucleus is unstable and decays into nucleons and fragments or undergoes fission.

Problems of the dynamics of highly excited nuclear matter attract much attention. The investigation of nuclear systems with high excitation energies became possible owing to the creation of relativistic ion beams at the SP. The possibility arose of formulating and solving the problem of limit excitation energy and temperature achievable in a nuclear system. To describe processes in this region, the evaporation model is not sufficient because it does not take the production of secondary particles in the $E > 20$ MeV region into account. In order to describe the interaction of protons and light nuclei with heavy nuclei at beam energies exceeding ~ 1 GeV, cascade models are being developed in which fast particles are produced as a result of nucleons of the beam particle undergoing multiple scattering by nucleons of the target nucleus. A coalescence model exists in which secondary particles with close momenta stick to each other. There are also hydrodynamical, statistical, and thermodynamical algorithms; however, their use is limited because they involve free parameters.

A number of models have been developed for the description of excited nuclei. The fragmentation mechanism due to a gas–liquid phase transition is considered, as is the decay of a nuclear lattice, etc.

In the 1980s, a large number of studies were carried out with the SP and other devices with the purpose of developing models and identifying details of the nuclear fragmentation mechanism. A 'spectrometer of recoil nuclei' (SRN) was installed in the internal SP beam. Mobile telescopes composed of silicon semiconductor detectors were placed inside the accelerator chamber [40]. A typical telescope layout is shown in Fig. 7. The telescopes could be shifted within a range of angles between 45° and 135°. Charged particles landing in the aperture of a telescope were identified by the $\Delta E - E$ method, where ΔE is the energy registered by one or several first-line detectors and E is the remaining energy registered by the last-line detectors. Only particles stopping in the telescope are identified correctly. An example of the distribution of $\Delta E - E$ signals is presented in Fig. 8.

Figure 9 shows the mass spectrum of C−Si fragments registered by a telescope. This telescope registers isotopes in the energy range from 1 up to 50 MeV per nucleon.

Measurements of inclusive differential production cross sections of fragments with $Z = 5-12$ in reactions $p + Au \rightarrow Z + X$ and $He + Au \rightarrow Z + X$ carried out with SRNs are presented in [41] (Fig. 10). Z particles are registered within the range of angles between 35° and 135°. The beam energy ranges from 1.3 to 13.5 GeV.

Fragment production is conventionally considered to proceed from the highly excited matter of the residual

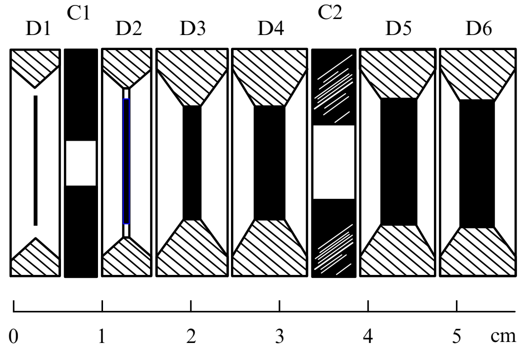

Figure 7. Telescope composed of six silicon semiconductor detectors (SSDs), installed in the SP vacuum chamber. D1–D6 — SSDs of thicknesses 10, 50, 100, 300, 1000, and 1000 μm. C1 and C2 — collimators.

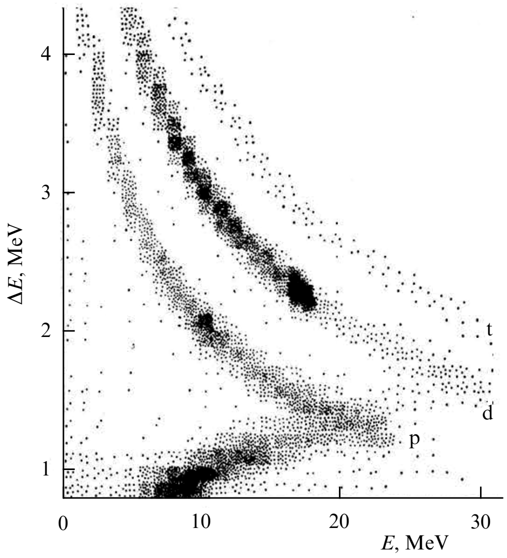

Figure 8. Distribution of $\Delta E - E$ signals in a semiconductor telescope and identification of hydrogen isotopes p, d, t. The enhanced concentration of points on the p and d curves corresponds to peaks in elastic p–p- and p–d-interactions in the deuterated polyethylene film target.

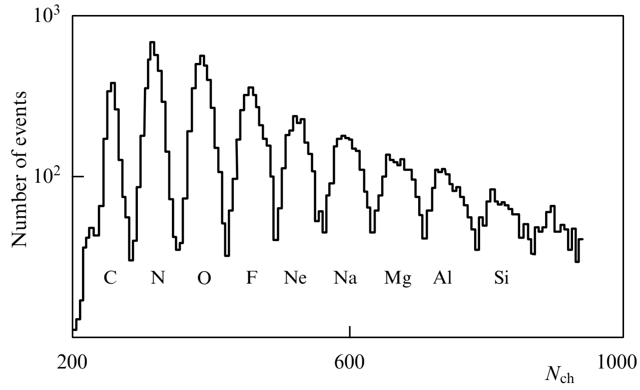

Figure 9. Mass spectrum of nuclear fragments registered by the semiconductor telescope.

nucleus undergoing a gas–liquid phase transition. Fragments are emitted when the nuclear system formed as a result of primary heating and compression expands and turns out to be in the vicinity of the critical point. The critical point in the density–temperature phase diagram is characterized by density fluctuations covering the entire system volume. In this state, an exponential dependence of the fragment production cross section on the fragment mass or charge should be observed. To verify this concept, the total cross sections of fragment production were determined and approximated by the dependence $\sigma(Z) \sim CZ^{-\tau}$, where C is a constant and τ is a dimensionless parameter characterizing the charge, Z, and mass, A ($Z \sim A$), distributions of fragments. In the case of the ^{4}He + Au reaction, a minimum of the function $\tau(E_{^4\mathrm{He}})$ is at $E_{^4\mathrm{He}} \approx 6$ GeV (Fig. 11). This points to the system having reached the phase transition condition.

Data on the angular dependence of fragment production permit finding the moving reference frame in which the angular distribution of particles in a given energy interval is isotropic. The cross sections were analyzed in the framework of a model assuming the existence of two sources of fragments moving with different transfer velocities. The slow source has the velocity $\beta = (2 \pm 0.7) \times 10^{-2}$ and the fast one has $\beta = (5 \pm 0.7) \times 10^{-2}$. From Fig. 11, the nonmonotonic behavior of the parameter $\tau(E_{^4\mathrm{He}})$ is related to the decay of the fast source.

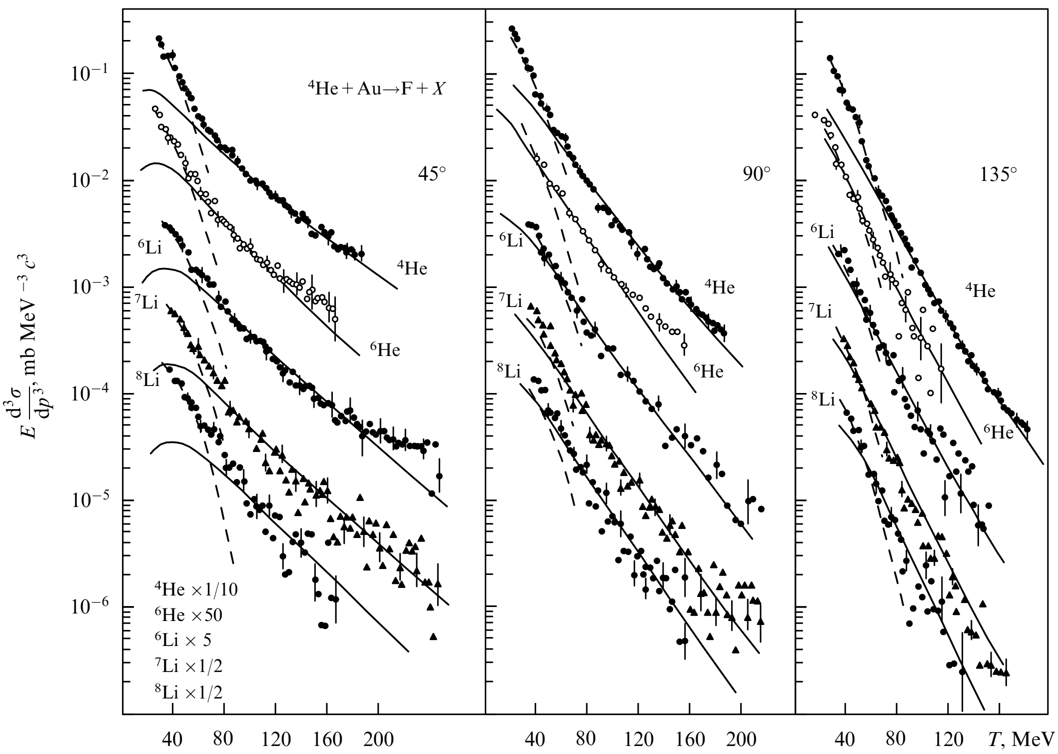

Figure 10. Example of differential production cross sections of fragments registered by the SRN device. The dashed lines are the results of calculations with the thermodynamical evaporation model. The solid lines are the results of calculations with the model with two moving sources of fragments.

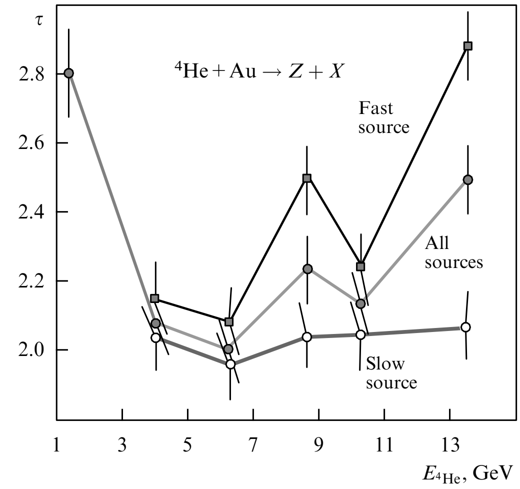

Figure 11. Dependence of the parameter τ on the ^{4}He beam energy.

Studies of nuclear fragmentation continued at the SP with the Faza device, which is a hybrid scintillation spectrometer with a registration angle close to 4π [42. 43]. In Ref. [44], the measurement of the gas-liquid phase transition critical temperature is presented. The value obtained for the critical temperature is 17 ± 2 MeV. These studies are still underway at the Nuclotron of the Veksler and Baldin Laboratory of High Energy Physics (LHEP), JINR.

The SP and Nuclotron age substantially enriched our knowledge of the structure of matter. Experimental instruments and methods also underwent significant development. A higher level of international collaboration among scientists was also achieved. The corresponding studies repeatedly won state prizes.

2. New physics in the collisions of heavy nuclei

The analysis of experimental data and numerical simulation of QCD processes in [45] revealed that the possible state of nuclear matter reaching the limit temperature and 'net baryon density' (NBD) — the density difference between baryons and antibaryons produced in collisions of ions — can be obtained in collisions of heavy nuclei at relativistic CMS energies $\sqrt{s_{NN}} \sim 10$ GeV (Fig. 12). In 2005–2006, work started at JINR on the design of a heavy-ion collider for this energy range [46, 47].

As the energy of colliding heavy nuclei increased, evidence was obtained in a number of CERN and BNL experiments of the formation of a particular state of hot and dense nuclear matter, the quark–gluon plasma (QGP). A (hypothetical) phase diagram was plotted of the possible states of matter produced in a collision of two heavy nuclei. Figure 13 shows the present-day version of the diagram [48].

The diagram reflects the results of simulation: the most interesting temperature–density range promising 'new physics' is the region of the hadron matter transition to the state of quark–gluon matter via a mixed phase, which can be achieved precisely in the energy region indicated. At the same time, in collisions at superhigh energies at RHIC (Relativistic Heavy Ion Collider) and LHC, the formation of hot matter with a low NBD occurs. The mixed-phase domain in the diagram has a limited size. The mixed phase with a relatively low NBD and high temperature comes to an

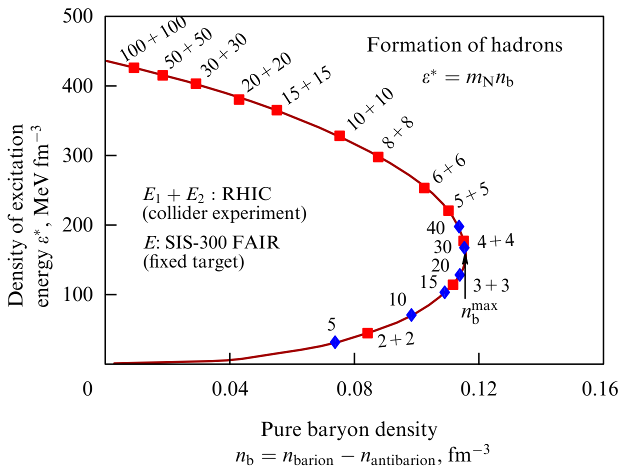

Figure 12. Result of the analysis of the parameters of nuclear matter produced in collisions of heavy nuclei: dependence on the collision energy of the excitation energy density (proportional to temperature) and of the 'net baryon density' — the difference between the densities of baryons and antibaryons [28]. Squares indicate the energy $E_1 + E_2$ of collider particles; diamonds indicate the particle energy E in a fixed-target experiment.

end at the so-called critical point, above and to the left of which only a second-order phase transition is possible with density and other parameters changing continuously — a so-called crossover. As the collision energy decreases, a mixed phase arises, which reaches a bifurcation point below and to the right. Here, the mixed phase region splits into two, between which lies a 'quarkion phase'; exotic matter is expected to emerge in this region.

According to modern ideas, the state of matter whose investigation will be possible in heavy-ion collisions at the NICA collider existed in Nature at approximately the first microsecond after the Big Bang. Such a fascinating problem could, naturally, not be left without the attention of other world laboratories. The following laboratories are competitors and at the same time partners of JINR in this research: CERN, Brookhaven National Laboratory (USA), and the Helmholtz Center for Studies of Heavy Ions (GSI) with the project Facility for Antiproton and Ion Research (FAIR) (Germany) (Fig. 14).

3. NICA accelerator complex

The new NICA accelerator complex [49] will permit implementing experiments in the following modes:

(1) with the Nuclotron ion beams extracted to a fixed target;

(2) with colliding ion beams in the collider at kinetic energies in the range 1–4.5 GeV per nucleon;

(3) with colliding proton–ion beams in the same energy range;

(4) with colliding beams of polarized protons (5–12.6 GeV) and deuterons (2–5.8 GeV per nucleon).

The NICA complex (Fig. 15) includes the following main elements:

— an injection complex;

— a superconducting synchrotron, *Booster*;

— the superconducting synchrotron, *Nuclotron*;

— a *Collider* composed of two superconducting rings with two beam intersection points;

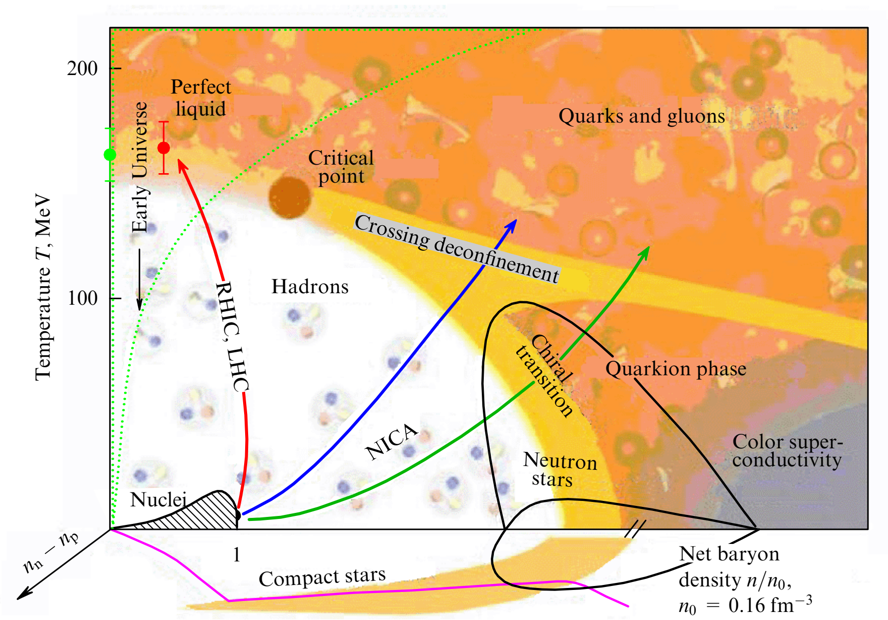

Figure 13. Phase diagram of strongly interacting matter [31]: the dependence of the temperature of the system of two colliding nuclei on the net baryon density (in units of the nuclear matter density n_0).

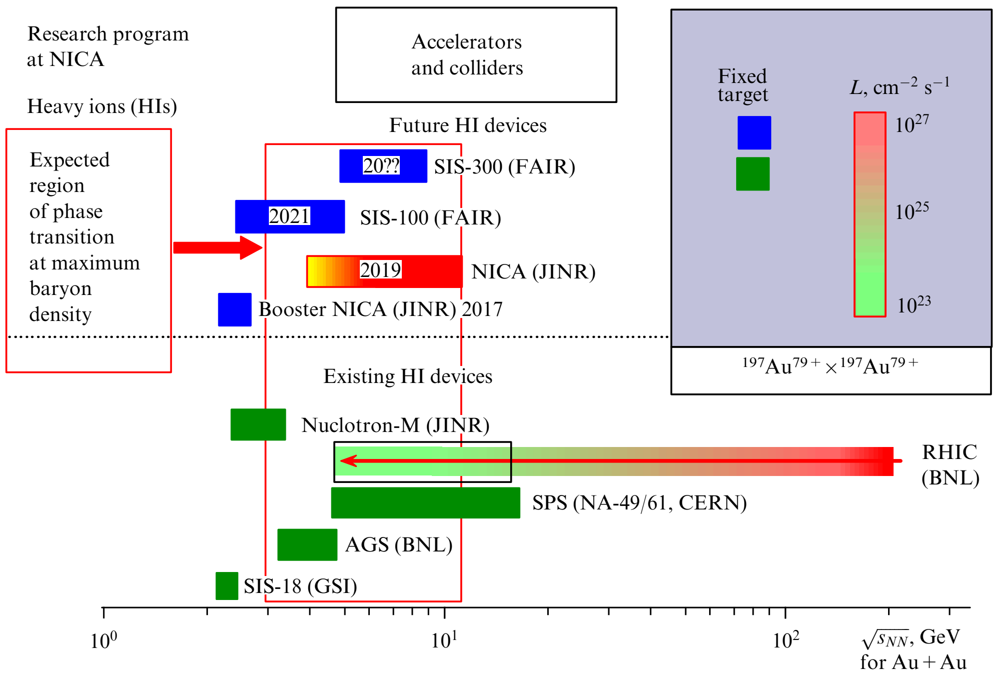

Figure 14. (Color online.) Heavy-ion accelerators and colliders in laboratories performing or preparing studies of baryon matter in heavy-ion collisions. Blue or green color indicates an accelerator generating beams extracted to fixed targets; in this case, the luminosity L is limited by the detector efficiency; red–yellow color indicates colliders whose luminosities ('color') change with energy in accordance with the color scale presented in the upper right part of the figure.

— two detectors: a Multi-Purpose Detector (MPD) and a detector for experiments in particle spin physics, the Spin Physics Detector (SPD);

— channels for beam transportation.

The tasks for the NICA project also include creation of a control system for the accelerator complex and development of a cryogenic complex and the laboratory infrastructure.

The creation of the accelerator complex and implementation of its physics program are divided into several stages:

— developing the injection complex, constructing the Booster, and performing fixed-target experiments;

— constructing the Collider and its operation with colliding heavy-ion beams of particles of the same sort;

— upgrading the beam intersection segment for the realization of operation with colliding beams of different kinds of ions and equal energies per nucleon (in this case, the magnetic rigidities of the Collider rings are different);

— equipping the Collider rings with devices for particle spin control and polarized beam diagnostics, performing

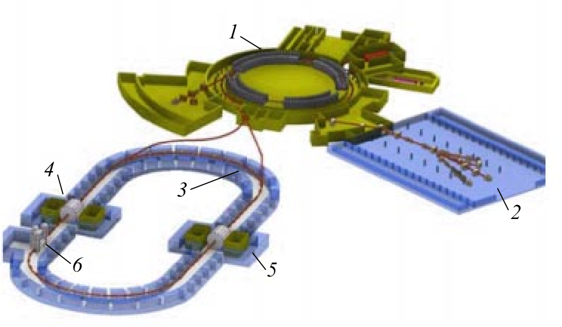

Figure 15. Layout of the NICA complex: *1* — building that houses the injection complex, the Booster, and the Nuclotron, *2* — existing building for fixed-target experiments, *3* — Collider, *4* and *5* — MPD and SPD detectors, *6* — electron cooling system (ECS) of the Collider

experiments in spin physics with colliding beams of polarized particles.

The *injection complex* includes a set of ion sources and two linear accelerators. The first one, the LU-20 linear accelerator, which is in operation, accelerates protons and ions from the sources: a laser source, a duoplasmotron, and a source of polarized protons and deuterons (Source of Polarized Ions, SPI). At the LU-20 exit, the energy of ions is 5 MeV per nucleon ($A/Z = 3/1$). At present, the LU-20 beam is injected directly into the Nuclotron.

The second accelerator — a new heavy-ion linear accelerator (Heavy Ion Linac, HILAc) — is at the stage of assembling and commissioning. It will accelerate heavy ions ($^{197}Au^{31+}$ ions have been chosen as the base ions) injected from KRION, a superconducting (SC) electron-string heavy-ion source. The energy of ions at the exit from HILAc is 3.2 MeV per nucleon, while the beam intensity amounts to 2×10^9 particles per pulse.

The *Booster* is a superconducting synchrotron intended for accelerating heavy ions to an energy of 600 MeV per nucleon. The magnetic structure of the Booster with a 211-m-long circumference is established inside the yoke of the synchrophasotron magnet. Ions accelerated in the Booster are extracted and transported along a superconducting magnetic *channel*, and on their way they cross a *stripper target*, inside which they are ionized to the maximum-charge state ($^{197}Au^{79+}$ in the case of gold).

The upgraded *Nuclotron* accelerates protons, deuterons (also polarized deuterons), and ions to a maximum energy depending on the sort of particles (Table 1).

The *Collider* consists of two storage rings with two interaction points (IPs). Its main parameters are as follows: the magnetic rigidity is up to 45 T m; the residual gas pressure in the beam chamber is not higher than 10^{-10} Torr; the maximum field in dipole magnets is 1.8 T; the kinetic energy of gold nuclei ranges from 1 to 4.5 GeV per nucleon; the beam axes coincide at the intersection segment (zero intersection angle); and the average luminosity is 10^{27} cm^{-2} s^{-1} for gold ions at $\sqrt{s_{NN}} = 11$ GeV. The rings of the Collider are identical in shape to a racetrack: two arcs are connected by two long straight sections (109 m each). The circumference of each ring is 503.04 m (the doubled Nuclotron perimeter). The dipole magnets and lenses in the arcs are combined into 12 cells of the so-called FODO structure separated by straight (small) gaps. The magnets of both rings in the arcs are situated one above another; their axes are separated vertically by 320 mm. The magnets in the arcs have common yokes, but their

Table 1. Main parameters of the NICA accelerator complex.

Parameter	Booster	Nuclotron
Type	SC synchrotron	SC synchrotron
Particles	Ions, $A/Z \leqslant 3$	p$\uparrow$, d$\uparrow$, nuclei
Injection energy, MeV per nucleon	3.2	5 (p$\uparrow$, d$\uparrow$), 570–685 (gold nuclei)
Maximum energy, GeV per nucleon	0.6	12.07 (p$\uparrow$), 5.62 (d$\uparrow$), 4.38 (gold nuclei)
Magnetic rigidity, T m	1.6–25.0	25–43.25
Perimeter, m	210.96	251.52
Cycle duration in the injection mode into the Collider, s	4.02 (active), 5 (total)	1.5–4.2 (active), 5 (total)
Leading magnetic field, T	0.11–1.8	0.03–2.03 (p$\uparrow$, d$\uparrow$) 0.46–2.03 (nuclei)
Field rising rate, T s^{-1}	1.2	1.0
Injection type	Single-turn, multiple-turn, multiple single-turn	Single-turn
Extraction type	Single-turn	Single-turn, slow
Residual gas pressure, Torr	10^{-11}	10^{-9}
Au beam intensity, number of ions per pulse	1.5×10^9	1×10^9
Duration of beam stretching in case of slow extraction, s	up to 10	up to 10

construction permits controlling the field in each of the rings separately. The beams are brought together and separated in the vertical plane. Upon passing the section bringing them together, the particle bunches of the upper and lower rings travel along a common straight trajectory toward each other to collide at two IPs. Single-aperture lenses are installed along these sections to provide the focusing of both beams at the IP (see Section 4).

The Collider will be built in a separate building with a tunnel for its rings, two chambers for detectors, and a room for the electron cooling system (ECS) (Figs 15 and 16).

4. Concept for achieving the project luminosity of the NICA collider

The high luminosity of the Collider implies, first of all, the generation of beams of high density and intensity at all stages of their formation and of particle acceleration. For this, the Booster is equipped with an electron cooling system that can provide ion accumulation at the injection energy (3.3 MeV per nucleon, the electron energy being 1.8 keV) and cooling of accelerated particles at a certain intermediate energy (100 MeV per nucleon and 54.5 keV) (Fig. 17). The application of electron cooling, reducing the six-dimensional phase-space volume of the beam of cooled particles (emittance), opens the possibility of multiple ion injection into the Booster, which relaxes the requirements to the injected beam intensity (the KRION–HILAc chain). Cooling at the inter-

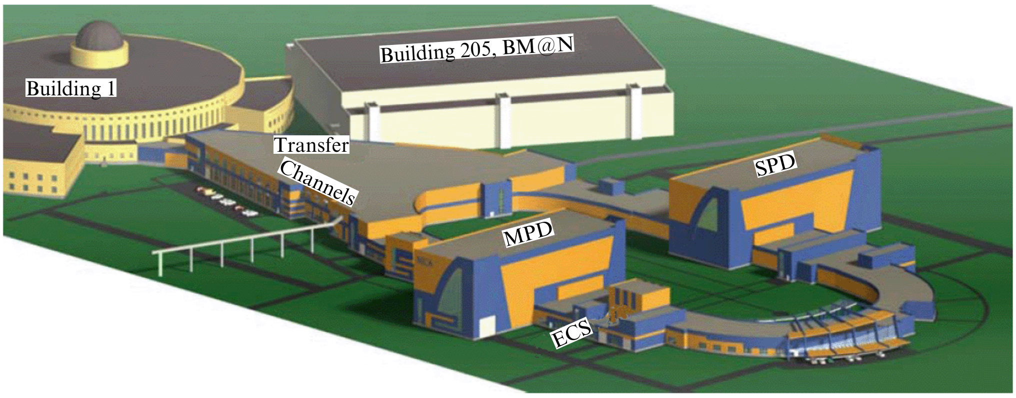

Figure 16. Accommodation of the NICA complex on the territory of the LHEP, JINR.

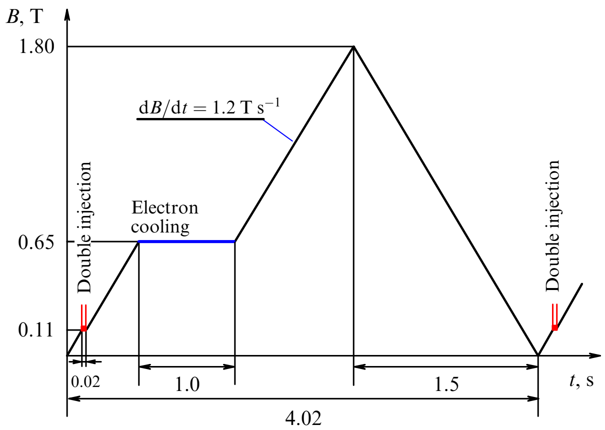

Figure 17. Diagram of the Booster operation. B is the magnetic field in the dipole magnets of the Booster.

mediate energy permits minimizing the transverse size of the beam of accelerated particles and their energy spread. This is necessary for the effective extraction of accelerated particles from the Booster for fixed-target experiments and/or their transfer to the Nuclotron.

The design and parameters of the Booster ECS are quite typical for such low-energy devices: the cooling section is 4 m long and the electron beam current is up to 1 A, which provides a cooling time of 1 s at the maximum electron energy of 54.5 keV. The ECS was designed and constructed at the Budker Institute of Nuclear Physics (INP), Siberian Branch, RAS.

Particles in the channel for transportation from the Booster to the Nuclotron pass through a thin target (graphite or a copper foil 100 μm thick). There, 90% of the $^{197}\mathrm{Au}^{31+}$ ions are completely stripped. The $^{197}\mathrm{Au}^{79+}$ nuclei are injected into the Nuclotron, where they are accelerated to energies of 1.0–4.5 GeV per nucleon. Then the ions are transferred to the Collider, where they are accumulated and the beam is shaped into short bunches. As is explained below, this is necessary for achieving the desired luminosity. In the case of identical colliding bunches of circular cross sections, the peak luminosity is given by

$$L = \frac{N_{\mathrm{b}}^2}{4\pi\varepsilon\beta^*}\, F_{\mathrm{coll}}\, f_{\mathrm{HG}}\left(\frac{\sigma_{\mathrm{s}}}{\beta^*}\right), \qquad (5)$$

where N_{b} is the number of ions in a bunch, ε is the transverse, unnormalized (geometric) root-mean-square emittance of the bunch, β^* is the value of the Collider betatron function at the IP (a characteristic of its focusing system, the transverse beam dimension, proportional to the square root of β^*), σ_{s} is the root-mean-square bunch length, F_{coll} is the collision frequency equal to the ratio of the particle velocity to the distance between bunches in the ring, $f_{\mathrm{HG}} \leqslant 1$ is a parameter describing the decrease in luminosity occurring as the bunch length increases (the so-called 'hour-glass' effect), and the value of f_{HG} is close to unity when $\sigma_{\mathrm{s}} \leqslant \beta^*$. Hence, it can be seen that short intense bunches of small transverse size are required [the $\varepsilon\beta^*$ factor in formula (5)]. The design values in the NICA collider are $\sigma_{\mathrm{s}} = 60$ cm and $\beta^* = 35$ cm.

For ion accumulation and the formation of ion bunches with the necessary parameters in the Collider, three systems of the acceleration radio-frequency (RF) voltage will be used. Accumulation of a beam of the required intensity is planned to be realized in the longitudinal phase space with the use of the 'technique of barrier RF voltages' and of stochastic or electron cooling of the particles being accumulated. When the necessary intensity is achieved, the beam is bunched by the RF system of harmonic voltage of the 22nd harmonic of the rotation frequency with the subsequent takeover by the RF system of the 66th harmonic. This permits 22 short bunches to be formed, which is necessary in order to achieve high luminosity.

To maintain the required luminosity level during the experiment, it is necessary to apply cooling methods. When the experiment is being performed, a decrease in the luminosity may be caused by two processes: a loss of particles and an increase in the phase volume of the bunch.

An increase in the beam phase volume is due to the influence of many combined effects: multiple scattering on atoms of the residual gas, noise of the power supplies of elements of the Collider magnetic system and, for the RF-resonators, intrabeam scattering (IBS), the crossing of non-linear high-order resonances by particles, etc. To stabilize the phase volume of a bunch, stochastic or electron beam cooling is used, which results in equalizing all the effects of heating. In the case of such equilibrium between cooling and heating processes, the luminosity lifetime depends only on the lifetime of the particles.

Of all the effects leading to a direct loss of particles, the most significant ones are single scattering by large (aperture) angles on atoms of the residual gas and, in the case of electron cooling, recombination with the cooling electrons. The vacuum conditions in the Collider provide a beam lifetime related to scattering by the residual gas, of the order of several hours. The project beam accumulation time in each ring is about 2–3 min. Therefore, if the time chosen for the experiment is optimal, the mean luminosity is close to the peak value.

In the case of the electron cooling of heavy-ion beams, one of the most serious problems is the recombination of ions with electrons of the cooling beam. The capture of an electron by an ion in the cooling section results in a change in the charge state and, thus, to the ion being lost due to a change in the position of its orbit. The recombination rate depends weakly on energy (the process occurs in a reference frame moving at the mean velocity of the ions and the cooling electrons). The possibility is being considered of suppressing recombination by increasing the temperature of the transverse degree of freedom of the electrons [50]. This may be achieved by different methods: by the adiabatic compression of the electron beam in the ECS magnetic field increasing with the distance from the electron gun toward the cooling section, by excitation of the Larmor rotation of the electrons via a transverse electric field at the exit from the gun and using a so-called hollow electron beam. The latter reduces the electron density at the beam center, where the ions already accumulated circulate, leaving the density sufficiently high at the beam edge, where new injection occurs. It is also quite effective as regards shifting the electron beam energy with respect to that of the ion beam.

The maximum number of bunches $n_{\max}$ is restricted by the minimum possible distance between them, the choice of which is based on the requirement that there be no parasite collisions between the bunches of colliding beams in the section where the beams overlap in the IP vicinity. In the NICA collider, $n_{\max} = 22$. It is preferable to have an even number of bunches in a ring in order that simultaneous registration of the results of bunches colliding at both IPs be also possible. This is necessary for controlling operation of the Collider and of both detectors.

Another restriction on the number of bunches is due to the so-called electron cloud effect: the accumulation of electrons in the electric field of the beam circulating in the collider. This effect can result in a loss of ions undergoing charge exchange in electron 'clouds'. Calculations show that the beam parameters in the NICA collider are somewhat lower than the formation threshold of 'clouds' (for details, see Ref. [51]).

As was mentioned above, Collider luminosity (5) increases as the bunch length decreases. The peak beam current, however, increases in this case, which leads to an increase in the shift of betatron oscillation frequencies and to coherent (microwave) beam instability. As a compromise between the two opposite requirements — of beam stability and of reaching the design luminosity — the root-mean-square bunch length was chosen to be equal to 60 cm.

The threshold of coherent bunch instabilities also increases with the spread of particles in momentum. At the same time, this does not lead to a decrease in the luminosity (the dispersion of the collider magnetic system at both IPs is zero). Therefore, to achieve maximum luminosity, the momentum spread must be chosen as large as is allowed by the restrictions related to the longitudinal acceptance and the technically achievable RF-voltage amplitude necessary for bunch formation (retaining). In the NICA collider, the root-mean-square relative momentum spread $\Delta p/p < \pm(1-1.5) \times 10^{-3}$ (1/6 of the acceptance) seems quite acceptable. The required RF-voltage amplitude at the 66th harmonic does not exceed 1 MV.

As mentioned above, the main sources of heating are IBS and, in the case of a large betatron frequency shift ΔQ_{sc}, high-order nonlinear resonances. In the NICA collider, two limit operation modes are distinguishable: the IBS-dominated mode and the space-charge-dominated (SCD) mode. In the IBS-dominated mode, the longitudinal and transverse phase space volumes are coupled to each other, and the minimum rate of heating for a given momentum spread corresponds to a rigorously defined emittance value. In the SCD mode, the enhancement rates of the phase space volume are significantly higher. But the nature of heating differs essentially in the cases of longitudinal and transverse degrees of freedom, and the bunch emittance can be chosen independently of the particle momentum spread. As a result, compensating the beam heating in the IBS-dominated mode requires significantly lower cooling rates, and is therefore preferable in the case of large ion energies, when it is much easier to achieve the design luminosity by using *stochastic cooling*. At low energies, the possibility of increasing the luminosity is related to passing to the SCD mode, while the required high cooling rate can be provided by applying *electron cooling*. Both cooling methods are used in the NICA project based on new technology achievements (see Section 6).

It must be stressed that the collider luminosity essentially depends on the energy of colliding particles. This dependence enters formula (5) via all the parameters involved in it. This is manifested most strongly in the restriction of the particle number per bunch N_{b}, whose maximum value for relativistic particles is inversely proportional to the energy cubed. In the case of heavy ions, one more restriction arises: $(N_{\mathrm{b}})_{\max} \propto A/Z^2$, where A is the atomic weight of the nucleus and Ze is its charge. Therefore, the luminosity of ion–ion colliders in the range of NICA energies is much lower than the luminosity of proton–proton colliders.

5. Detectors at the NICA complex

5.1 BM@N experiment

The purpose of the Baryonic Matter at Nuclotron (BM@N) experiment [52] is the investigation of dense baryonic matter with a beam of relativistic heavy ions extracted from the Nuclotron to a fixed target. In such experiments, the heavy-ion beam intensity $\mathrm{d}N_{\mathrm{ion}}/\mathrm{d}t$ may be much lower than planned for collider experiments because in this case the luminosity

$$L_{\mathrm{fixed}} = n_{\mathrm{t}} d_{\mathrm{t}} \frac{\mathrm{d}N_{\mathrm{ion}}}{\mathrm{d}t} \tag{6}$$

is proportional to the target density n_{t} and thickness d_{t}. In the case of a solid-state (foil, film) target, the value of $n_{\mathrm{t}} d_{\mathrm{t}}$ can be of the order of 10^{19} cm^{-2}, which for a flux of 10^8 ions per s yields the desired value 10^{27} cm^{-2} s^{-1}. We note that such a scheme was considered at the beginning of discussions of a project aimed at searching for a 'mixed phase', but it was soon discarded owing to significant advantages of the collider version. Nevertheless, the BM@N experiment, which is a new 'reading' of the initial version of the project, permits starting studies within the next two years after commissioning

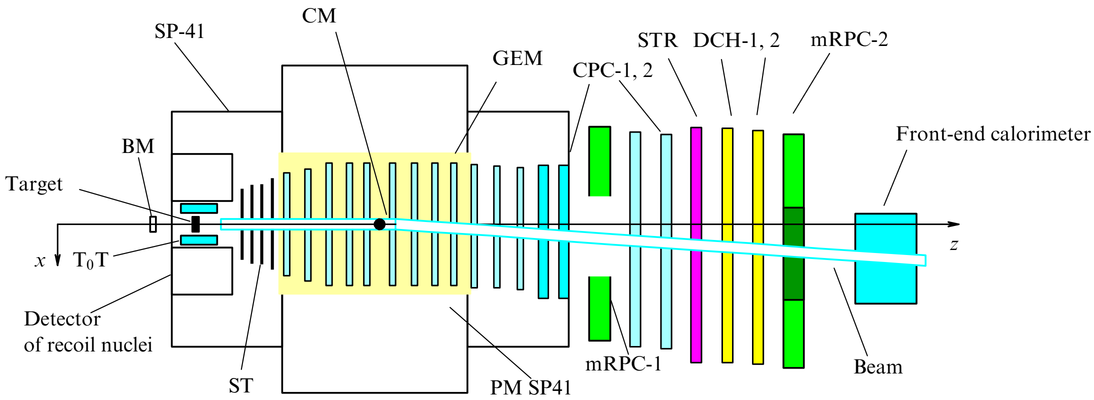

Figure 18. Layout of the BM@N setup: GEM — central tracker in the aperture of the analyzing magnet; T_0T — trigger and start counter T_0; BM — beam monitor; SP-41 — spectrometric magnet; ST — microstrip silicon detector; CM — spectrometric magnet; CPC-1, 2 — proportional chambers with cathode readout; DCH-1, 2 — drift chambers; PM SP41 — pole of magnet; STR — straw tracker, a — gas-filled coordinate detector consisting of a set of mylar tubes ('straws') 4–10 mm in diameter and 2.5 m long, along the axis of each tube of which a metal wire about 25 μm in diameter is tightened; the ionizing particle coordinate is determined by the point at which a discharge occurs between the wire and the metal coating of the tube; mPRC-1, 2 — multigap planar chambers that, together with the subdetector T_0T, serve as a time-of-flight system.

Figure 19. BM@N detector in the experimental hall at the channel of beams extracted from the Nuclotron (the wide-aperture analyzing magnet is seen in the central foreground; on the left are hexagonal proportional chambers; on the right the steering magnet is seen on the beam entrance trajectory).

of the KRION–HILAc–Booster injection chain, with the acceleration of $^{197}Au^{79+}$ nuclei in the Nuclotron to an energy of 4.5 GeV per nucleon ($\sqrt{s_{NN}} = 3.47$ GeV).

Commissioning of the BM@N detector (Figs 18 and 19) was initiated earlier, in March 2015, before commissioning of the Booster, with the use of the injection chain involving the Duoplasmotron ion source (or plasma source), LU-20, and acceleration in the Nuclotron of heavy ions, up to Xe inclusive ($A/Z = 3/1$), to 3.5 GeV per nucleon ($\sqrt{s_{NN}} =$ 3.19 GeV) at a significantly reduced intensity. The BM@N experiment will be carried out in collaboration with group of the FAIR project, in which a similar experiment is planned with the beam extracted from the SIS-100 synchrotrons to a fixed target, $E_{\mathrm{kinetic}} = 1-11$ GeV per nucleon, $\sqrt{s_{NN}} =$ $2.33-4.97$ GeV, and later from SIS-300, with $E_{\mathrm{kinetic}} =$ $10-35.36$ GeV per nucleon and $\sqrt{s_{NN}} = 4.7-8.4$ GeV (see Fig. 14).

The physics program to be implemented with the BM@N setup includes the following tasks.

(1) Studies of heavy-ion collisions ($A + A$ collisions) for investigating the properties of dense (mainly baryonic) matter with strangeness, namely:

• hadron production mechanisms and modification of their properties in dense nuclear matter (used as test probes are the production of strange mesons, strange and multi-strange baryons, and vector mesons in hadron, dilepton, and/or photon channels);

• equations of state of nuclear matter with strangeness;

• the search for light hypernuclei and multistrange metastable objects (hypermatter).

(2) Obtaining data on the 'elementary' reactions pp and pn(d) to reveal nuclear effects.

(3) Investigation of 'cold' nuclear matter in $p + A$ collisions.

At its initial stage, the BM@N experiment will study effects due to the influence of the medium on strangeness by measuring observables at different energies and degrees of centrality in heavy-ion collisions with the aim of revealing anomalies in the regularities predicted by theoretical models. The observables sensitive to these effects are the production cross sections of different particles, the mass distributions of secondary particles with respect to the transverse momentum component, their rapidity distributions (angular distributions), and collective particle fluxes (jets). In the future, it will be possible to investigate medium effects in the production of vector mesons ($V = \rho, \omega, \varphi$) in the dilepton channel $V \to e^+e^-$, or the photon one, $\omega \to \gamma\pi^0$, and also in the decay channel $\varphi \to K^+K^-$.

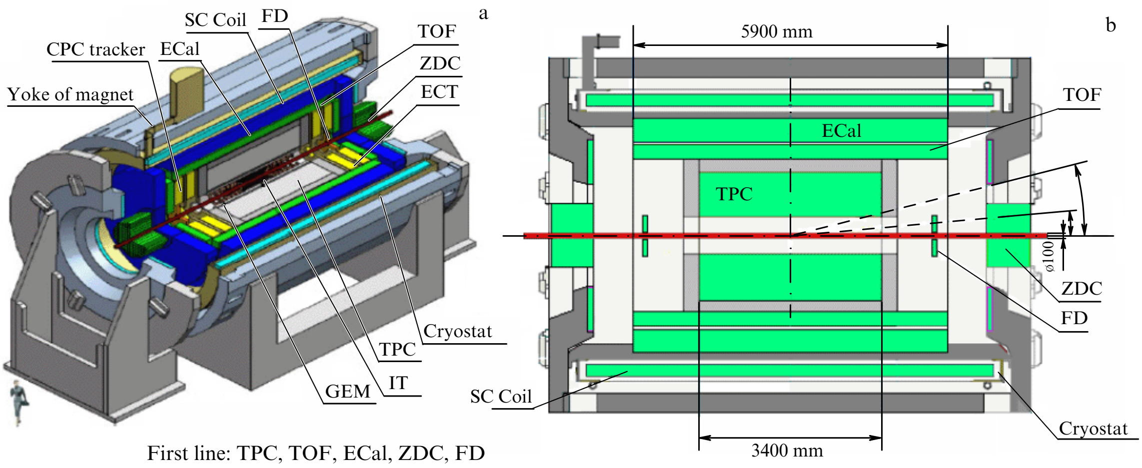

Figure 20. (a) MPD detector for experiments with the NICA collider. (b) Elements of the first detector stage. SC Coil — superconducting coil of solenoidal magnet, TPC — time-projection chamber, TOF — barrel part of the time-of-flight system, ECal — electromagnetic calorimeter, ZDC — calorimeter for particles emitted at small angles, FD — frontend calorimeter, IT — internal tracker, GEM (Gas Electron Multiplier) — coordinate detector based on gas electron multipliers, CPC tracker — tracker based on proportional chambers with cathode readout, ECT — endcap tracker.

Further development of the setup is planned: it is to be supplemented with a microstrip silicon vertex detector, with an electromagnetic calorimeter, and possibly with a neutron detector.

5.2 Multi-Purpose Detector

The Multi-Purpose Detector (MPD), whose design and construction pertain to the most large-scale and complex tasks of the project, is being created precisely to study the properties of hot and dense nuclear (baryonic) matter in heavy-ion collisions [52]. The problems of primary interest to be resolved first include the search for signals of possible phase transitions, of deconfinement, and of restoration of chiral symmetry, searching for the critical point, identifying the mixed quark–gluon phase of strongly interacting matter and studying the properties of hadrons in a medium, and formulating (refining) the equation of state of nuclear matter. Proposals of experiments for the MPD are collected in the NICA *White Paper* [48].

Solving these problems requires registering many characteristics of particles produced in ion collisions, of which the most informative are considered to be:

— ellipticity parameters of the flux of particles participating in the reaction in momentum space;

— parameters of the well-known 'horn effect' [53], which was observed in experiments where the dependence of the ratio of kaon and pion multiplicities $R(\theta) = \langle K^+\rangle/\langle\pi^+\rangle$ on $\sqrt{s_{NN}}$ was measured at the scattering angle θ close to 90° (the pseudorapidity $y^* \approx 0$). In the region $4 \leqslant \sqrt{s_{NN}} \leqslant 11$, the function $R(\theta \approx 0)$ exhibited a clear peak-like maximum;

— parameters of leptons and photons produced in the decays of mesons π, ρ, ω, φ, J/Ψ, and others. These leptons and photons carry information on the structure of the QGP produced in collisions and on its temperature;

— fluctuations of parameters of the products of collision reactions. These fluctuations are considered to be a signature of the mixed phase production (the classical analog is a fluctuating flow of bubbles in boiling water). In this case, the problem lies in registering and analyzing the fluctuations of (all!) the parameters of secondary particles, for example, of the dispersion and of higher moments of the $R(0)$parameter: $D_R = \left\langle (R - \langle R\rangle)^2 \right\rangle$, $M_{3R} = \left\langle (R - \langle R\rangle)^3 \right\rangle$, etc. In experiments at RHIC at $\sqrt{s_{NN}} \sim 200$ GeV, no fluctuations up to the 6th order were revealed, as was also the case at lower energies ($\sqrt{s_{NN}} \approx 15$ GeV), albeit owing to the low collider luminosity.

The MPD (Fig. 20) is a typical collider detector, consisting of a central (barrel) part and butt ends and end detectors, which are symmetric with respect to the central detector plane. The barrel and butt end parts of the detector are placed inside a large superconducting solenoid.

The MPD has the following main elements and units (subdetectors):

• a solenoidal magnet with the mean coil radius of 2.479 m and 7.535 m long, providing a magnetic field of 0.66 T with a homogeneity $\Delta B/B \leqslant 10^{-4}$ in the central part;

• toroidal magnets at the detector ends;

• a time-projection tracking 'chamber' — a TPC subdetector;

• a time-of-flight subdetector for particle identification (TOF-RPC) and a calorimeter for secondary particles emitted at small angles to the beam (ZDC). Reliable particle identification requires the particle time-of-flight measurement precision to be not worse than 100 ps. TOF-RPC, ZDC, and TPC together ensure precise measurement of particle momenta and their identification;

• an electromagnetic calorimeter (ECal), which together with the TPC ensures the identification of electrons;

• an internal tracker (IT) for the reconstruction of secondary vertices and identification of the relatively rare events of hyperon production with strangeness 2 or 3;

• trackers for particles emitted at small angles. These trackers are used in studies of fundamental effects related to the nonconservation of P and CP invariance;

• end detectors also used to identify particles emitted at small angles and to reconstruct the reaction plane.

The detector has a system for data acquisition, storage, and processing, which performs signal digitization, counting, and processing, resulting in an off-line reconstruction of the complete event topology.

During the 2009–2014 period, subdetector prototypes were designed and investigated for optimization of the

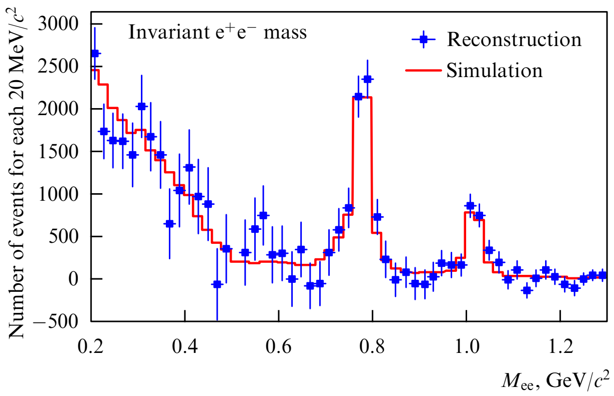

Figure 21. Reconstruction of lepton pair production at the MPD installation.

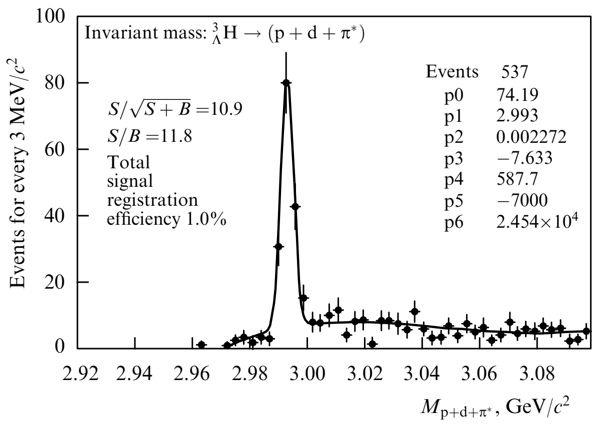

Figure 22. Simulation of the $^3_\Lambda$H hypernucleus yield at the MPD in the ^{3}Heπ^- channel. S and B are the signal and background intensities.

technical characteristics of the MPD setup (to achieve high registration efficiency and reconstruction accuracy of the parameters of particles produced in the whole range of solid angles).

Collision processes in the NICA collider were simulated for the MPD using the MpdRoot software package. This package, especially adapted for the MPD, is a version of the base software package FairRoot developed for the Compressed Baryonic Matter (CBM) experiment at the FAIR complex [52]. The data acquisition rate for Au + Au collisions at the maximum energy with a 10% sampling of central collisions was shown to be 7 kHz when the project average luminosity was $L = 10^{27}$ cm^{-2} s^{-1}. Hence, a total of 10^9 events can be planned to be collected in a week. Of the order of 10^8 of them are central events to be used in studies of femtoscopic correlations of particles with a strangeness greater than unity. For example, over 10^6 decays of Ω hyperons will be registered in a week of the Collider operation. The MPD provides reliable identification of charged particles by measuring the distribution of particle energy losses dE/dx in the TPC and the time-of-flight system. It was shown that quite a high resolution can be achieved in the interaction vertex reconstruction. Thus, in an analysis of the $\Omega \to \Lambda K^-$ decay channel in central Au + Au collisions at $\sqrt{s_{NN}} = 7.1$ GeV, the precision obtained was at a level of 10 μm. Special attention was paid to simulations of the possible detection of vector meson production in the dilepton decay channel. The results obtained (Fig. 21) confirm the possibility of reliable identification of these processes.

Optimal conditions for observing and studying light hypernucleus production processes have been provided both at BM@N and with the MPD detectors. For example, simulation results (Fig. 22) show an essential increase in the yield of single- and double-hypernuclei of hydrogen and helium in the energy range of the NICA collider.

6. NICA complex: a multifunction research laboratory. New accelerator technologies

The main program of experiments at the NICA complex, presented in Section 5, will be supplemented with various scientific and technological investigations, implementing which will require the use of accelerated particle beams. Without a doubt, the entire spectrum of particles in all of the accessible range of energies and with all available beam intensity levels will be of interest. The experience in such studies was acquired during the years of Nuclotron operation. Among these studies, the following must be mentioned:

— experiments in radiation biology, performed both with biomaterials and with animals [54];

— research in the framework of space programs, related to prolonged stays of human beings and of instrumentation in outer space;

— investigation of the fundamental possibility of creating nuclear energy facilities based on charged-particle accelerators [55].

Dedicated areas will be established in the NICA complex for implementing fundamental and applied research with beams of the injection complex and the Booster, and they will be extended to the Nuclotron beams.

The NICA complex, together with its accelerators and detectors, is an excellent 'workshop' for training skilled scientific and technical staff of high qualification, from students to the highest level of expertise. For this reason, the *JINR educational program*, which has already existed many years, takes significant advantage of the pedagogical opportunities arising due to the implementation of the project. Eleven base higher education departments of the following institutions function at JINR: Lomonosov Moscow State University, Moscow Institute of Physics and Technology (State University), National Research Nuclear University 'Moscow Engineering Physics Institute', and the University of Dubna.

Development of the NICA project is accompanied by the origination of various *accelerator technologies*. The first and best known is the technology for designing and constructing superconducting magnets for the Nuclotron [47], the Booster, and the Collider. They all have a design known as the 'Nuclotron type' (Fig. 23).

Magnets with yokes of laminated electrotechnical steel (the 'window frame' type for the dipole, and with poles of a hyperbolic shape for the quadrupole) and coils of a special superconducting cable, cooled by a flow of two-phase helium at the temperature $T = 4.5$ K, provide a magnetic field at the level of $B = 2$ T with the field variation rate dB/dt = 4 T s^{-1} and a cycle repetition frequency of 1 Hz [47]. The main element permitting the provision of such a unique rapidly

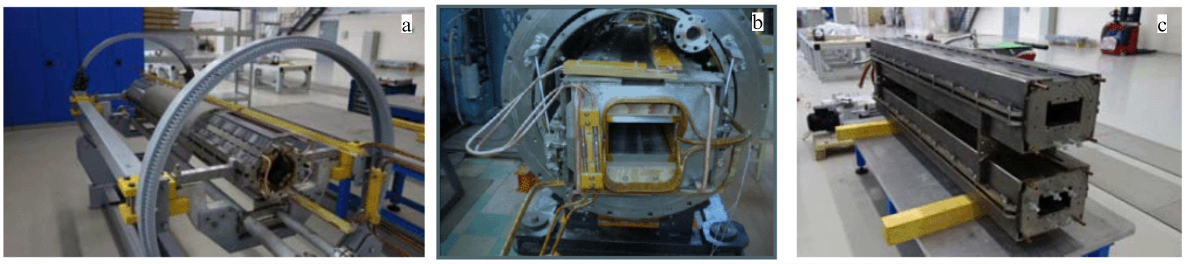

Figure 23. Serial magnets for the Booster: (a) doublet of quadrupole lenses, (b) dipole magnet, and (c) preserial two-aperture dipole magnet of the Collider (with one aperture above the other).

Figure 24. (a) Installation for testing SC magnets for NICA and FAIR projects, and areas (b) for SC cable production and (c) for manufacturing SC coils.

cycling operation mode of a superconducting device is a composite tubular Nb/Ti/Cu cable [56], proposed at the LHEP and exhibiting a minimum dynamic heat release together with a high superconductor cooling efficiency. Further development of the technology and upgrade of the 'Nuclotron type' magnets in 2000–2014 permitted the start of designing and constructing magnetic systems for the proton accelerators and the collider within the NICA project and for SIS-100 of the FAIR project (Germany) [57]. For this purpose, specialized production of such magnets was organized at the LHEP (Fig. 24).

Methods for cooling charged particle beams represent one of the key accelerator technologies that are critical for achieving the design parameters of the complex.

The *stochastic cooling system* (SCS) of the NICA collider must provide ion cooling of up to 2.3×10^9 ions in a bunch, which corresponds to an effective number 8×10^{11} of ions. To achieve the design cooling time, an SCS with the frequency band width 2–4 GHz is necessary. This corresponds to a range that has been well mastered in world practice and that presents no serious radiotechnical difficulties. The Collider SCS uses pickup electrodes and kickers of a new design: modular ring stations (Fig. 25), proposed and developed at the Institute for Nuclear Physics of the Jülich Research Centre (FZJ) (Germany) [58]. These devices underwent successful tests at the COSY (COoler SYnchrotron) storage ring at the FZJ and at the JINR Nuclotron [59], and they manifested their efficiency. They will be used for the cooling channels of horizontal and vertical degrees of freedom. Their design is envisaged to be optimized for the NICA collider: the aperture will be made smaller and the number of slots of the ring electrodes will be reduced.

The main elements of the stochastic cooling system also include signal delay system blocks, amplifier and preamplifier cascades, and a rejector (comb) filter system. Solid-state amplifiers will be used in the Collider SCS because they currently provide the best amplitude and phase characteristics. In practice, the achievable output power of one such

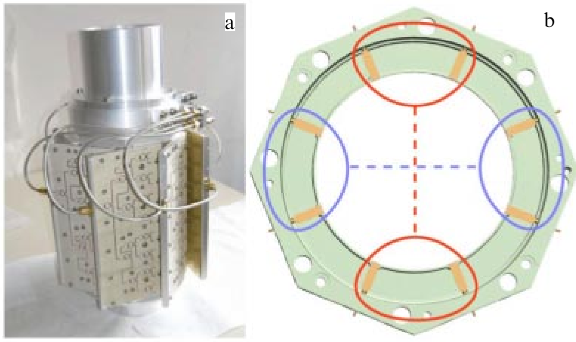

Figure 25. (Color online.) (a) Pickup station (set of 16 rings). (b) Combination of electrodes for measuring the horizontal (blue) and vertical signals of the beam amplitude.

device is about 60–70 W. Therefore, to provide the total required output power of the system at a level of 500 W, 8 to 10 kickers will be switched on in parallel, and each one of them will have an individual supply. An alternative consists in equipping each slot electrode (or group of slots) of the pickup station ring with its own low-power amplifier. In this case, the cost of the system can be significantly reduced, but the problem of matching the phases of such amplifiers arises. This version requires experimental testing at the Nuclotron SCS.

The block of optical delay lines (systems) and the optical comb filter (the instrumentation complex) was designed and successfully tested at the Nuclotron. The technological solution developed was chosen to be used in the Collider.

The *electron cooling system* for the NICA collider [60] is intended for accumulating ions of kinetic energies in the range 1.0–3.5 GeV per nucleon and for stabilizing the Collider luminosity at the required level in the operation mode of colliding beams in the entire working range of energies (1.0–4.5 GeV per nucleon). The results of numerical simulation of the evolution of beam parameters in the case of electron

Table 2. Parameters of the elecron cooling system of the NICA collider.

Parameter	Value
Electron energy, MeV	1.0 – 2.5
Energy stability, $\Delta E/E$	10^{-5}
Effective length of cooling section, m	6.0
Electron beam current I_e, A	0.1–1.0
Radius of electron beam, cm	0.5
Magnetic field in cooling section, T	0.2
Homogeneity of magnetic field	2×10^{-5}
Beta-function in cooling section, m, horizontal (center) vertical (center)	 11–13 13–14
Transverse electron temperature, eV	50.0
Longitudinal electron temperature, meV	5.0
Lifetime of ions due to recombination, h	$\geqslant 1.0$

cooling for technologically realistic ECS parameters (Table 2) points to the possibility of implementing this task.

The closest analog of the electron cooling system for the NICA collider is the ECS at an electron energy of 2 MeV developed at the Budker INR, the Siberian Branch, RAS for the COSY synchrotron and projected for HESR (High-Energy Storage Ring) (FZJ and FAIR project, Germany) [61]. In the course of development, the experience gained at the Fermi National Laboratory (FNAL) (USA) was also used: there, an ECS was successfully constructed and operated at an electron energy of 4.3 MeV [62]. Development of the ECS for the NICA collider is performed in collaboration with the Budker INR and the Lenin All-Russian Electrotechnical Institute (Moscow).

Two essentially different versions of the ECS are being considered (Fig. 26). In version a, developed at JINR, two independent electron-optical systems (EOSs) are created, permitting each of the two ion beams of the Collider to be cooled using its 'own' independent electron beam. Both EOSs use a common high-voltage power supply, but have independent power supplies for the electron guns and collectors. All these sources are housed in the middle tank and its 'head' that is under high voltage. The gun and accelerating tube of the first electron beam are in the left tank, from which the electron beam proceeds toward the cooling section of the lower Collider ring. Upon departing from it, the beam enters the right tank, where the accelerating tube of the first beam with the decelerating field is located, and ends with the electron collector. The EOS of the second beam, cooling ions of the upper ring, is arranged in a similar and mirror-symmetric manner. Electrons of both beams, slowed down in decelerating electric fields, enter their respective collectors. In this setup, the electrons of one of the guns travel from the cathode toward their collector along the magnetic field, while the electrons of the other beam travel in the opposite direction. A constant (accelerating) potential $U_{\rm coll} = 2-3$ kV is maintained between the cathode and the collector of each beam. As a result, the loss of power for recuperation of the beam is $P_{\rm coll} = I_{\rm e} U_{\rm coll} \leqslant 1.5$ kW.

In version b, proposed by the Budker INP, the accelerating and decelerating EOS of each of the two electron beams is inside its 'own' tank. Therefore, each of the two EOSs inside the tank has its own solenoid, which permits maintaining the field direction with respect to the electron velocity vector along the entire trajectory from the cathode to the collector (the fields of these solenoids are directed opposite to each other like the velocities of electrons in accelerating and decelerating accelerator tubes). Such a solution is used in the ECS of COSY. The overall dimensions in the ECS are minimized by using sectioned solenoids with sections 'hanging' according to the potential that is distributed along the tube.

A disadvantage of version b lies in a greater (about 20 m) length of the transportation solenoids compared with version a.

In version a, it may be relatively difficult to tune the electron energy recuperation mode in two beams whose EPSs have a common high-voltage power supply (0.5–2.5 MV).

The main feature of the ECS construction for the NICA collider is the use of superconducting solenoids, which permits significantly reducing power consumption by the ECS that cannot be avoided in the case of long solenoids used in the magnetic beam transportation system. The use of high-temperature superconductors (HTSCs) seems attractive. At present, HTSC tape 12 mm wide is produced by industry. The total length of HTSC tape required for the ECS solenoids in version a is about 20 km. Its cost in 2015 prices is 1.2 million US dollars (60 dollars per m) (the cost of HTSC tape tends to decrease as its production develops).

The *system for suppression of coherent transverse beam oscillations* [63, 64] (a feedback system, FBS) in the NICA collider is intended for:

— damping coherent transverse oscillations due to injection errors;

— suppressing coherent transverse instabilities;

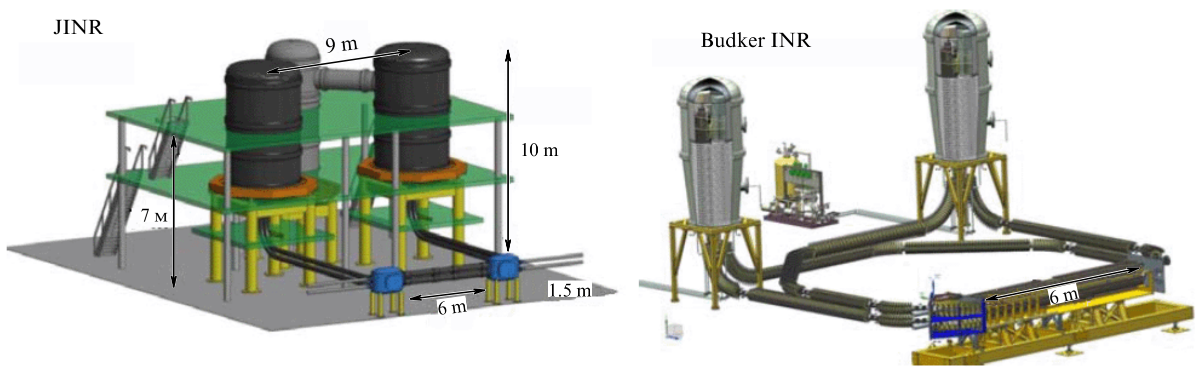

Figure 26. Two ECS versions for the NICA collider.

— exciting coherent transverse oscillations during measurement of betatron oscillation frequencies and beam response functions, and also for performing other measurements related to investigation of the transverse beam dynamics.

In developing the FBS for the NICA collider, the successful experience of the LHEP group in creating the FBS of the Large Hadron Collider was used.

Similar technological solutions were made in realizing the *system for cleaning the inter-bunch space* of background particles accumulating in the empty separatrices of the 66th RF-voltage harmonic. The necessity of creating such a system will arise when the design luminosity of the Collider is to be achieved.

The creation of the NICA complex required significant development of the *civil engineering infrastructure*. First of all, the doubling (from 4 to 8 kW) of the amount of cold produced at a temperature of 4.5 K must be noted. For this, the largest existing complex in Russia for liquid helium production, distinguished by a number of new efficient technological ideas and solutions [65, 66] was supplemented with a dedicated installation designed for liquefying helium and producing 1000 l in 1 h.

7. Conclusion

The NICA project has gone through the stages of conceptual and technological designing, and in September 2013 was approved by the Chief state expertise of the Russian Federation, which gave the official permission to start construction of the Collider building (see Fig. 16) and install infrastructural facilities. The plans for 2016–2017 are to upgrade the injection complex, to mount the Booster and put it into operation, and to upgrade the Nuclotron. The Collider, along with the beam transportation channel from the Nuclotron and the starting version of the MPD, should be constructed and put into operation by the end of 2019.

Creation of the NICA complex is possible only with broad international cooperation. Over a hundred theoreticians from 24 countries have already contributed to the development of the NICA scientific research program. Separate accelerating systems are under development with the participation of leading accelerator centers and institutions of the JINR member states: Russia (the Budker INR, RAS and ITEP, the National Research Center 'Kurchatov Institute'), Poland, the Czech Republic, and Bulgaria, and also CERN and research centers in Germany (GSI, FZJ, DESY) and the USA (FNAL, BNL), and others. The MPD, BM@N, and SPD experimental devices are being developed and constructed within the framework of international collaboration. A broad international collaboration permits using the most advanced technologies in creating installations, simulating the processes studied, and analyzing data. The NICA project complex has been submitted to a number of international expertise authorities and is constantly under control by international advisory councils during its creation.

A number of states have proposed introducing the project into the roadmap of the European Strategy Forum on Research Infrastructures, which is currently being upgraded. Having become part of the European research infrastructure, the NICA complex will open additional possibilities for attracting European research groups to carry out studies at its facilities.

References

1. Feinberg E L *Physicists. Epoch and Personalities* (Singapore: World Scientific, 2011); Translated from Russian: *Epokha i Lichnost'. Fiziki. Ocherki i Vospominaniya* (Moscow: Fizmatlit, 2003)
2. Vagin V A et al., in *Trudy Mezhdunar. Konf. po Uskoritelyam, Dubna, 21–27 Avgusta 1963 g.* (Proc. of the Intern. Conf. on Accelerators, Dubna, 21–27 August 1963) (Ed. A A Kolomenskii et al.) (Moscow: Atomizdat, 1964) p. 788
3. Zolin L S et al. *Sov. Phys. Usp.* **18** 712 (1975); *Usp. Fiz. Nauk* **117** 119 (1975)
4. Vovenko A S et al. *Sov. Phys. Usp.* **6** 794 (1964); *Usp. Fiz. Nauk* **81** 453 (1963)
5. Okonov E O, Podgoretskii M I, Khrustalev O A *Sov. Phys. JETP* **15** 537 (1962); *Zh. Eksp. Teor. Fiz.* **42** 770 (1962)
6. Nyagu D et al., Preprint P-2325 (Dubna: JINR, 1965)
7. Savin I A *Fiz. Elem. Chastits At. Yadra* **8** 28 (1977)
8. Aleksandrov Yu A et al. *Bubble Chambers* (Ed. N B Delone) (Bloomington: Indiana Univ. Press, 1967); Translated from Russian: *Puzyr'kovye Kamery* (Ed. N B Delone) (Moscow: Gosatomizdat, 1963)
9. Balandin M P et al. *Nucl. Instrum. Meth.* **20** 110 (1963)
10. Denisov S P, in *Trudy Mezhdunar. Konf. po Apparature v Fizike Vysokikh Energii, Dubna, 8–12 Sentyabrya 1970 g.* (Intern. Conf. on Instrumentation in High Energy Physics, Dubna, 8–12 September 1970) (JINR Publications, D-5805, Vol. 2) (Dubna: JINR, 1971) p. 615
11. Azimov Ya I et al. *JETP Lett.* **23** 114 (1976); *Pis'ma Zh. Eksp. Teor. Fiz.* **23** 131 (1976)
12. Azimov Ya I et al. *Yad. Fiz.* **3** 515 (1957)
13. Tolstov K D, Preprint No. 1698 (Dubna: JINR, 1964)
14. Zolin L S, Nikitin V A, Pilipenko Yu K, Preprint P-13-3425 (Dubna: JINR, 1967)
15. Zolin L S, Nikitin V A, Pilipenko Y K *Cryogenics* **8** 143 (1968)
16. Kang-Chang W et al. *Sov. Phys. JETP* **11** 977 (1960); *Zh. Eksp. Teor. Fiz.* **38** 1356 (1960)
17. Batyunya B V et al. *Nucl. Phys. B* **294** 1037 (1987)
18. Nikitin V A et al. *Yad. Fiz.* **1** 183 (1965)
19. Nomofilov A A et al. *Phys. Lett.* **22** 350 (1966)
20. Nikitin V A *Fiz. Elem. Chastits At. Yadra* **1** 6 (1970)
21. Nikitin V A *Fiz. Elem. Chastits At. Yadra* **10** 581 (1979)
22. Beznogikh G G et al. *Sov. J. Nucl. Phys.* **10** 687 (1969); *Yad. Fiz.* **10** 1212 (1969)
23. Bartenev V et al. *Phys. Rev. Lett.* **31** 1088 (1973)
24. Barbiellini G et al. *Phys. Lett. B* **39** 663 (1972)
25. Amaldi U et al. *Phys. Lett. B* **36** 504 (1971)
26. Kirillova L F et al. *Sov. J. Nucl. Phys.* **1** 379 (1965); *Yad. Fiz.* **1** 533 (1965)
27. Astvacaturov R G et al. *Phys. Lett. B* **27** 45 (1968)
28. Tsyganov E N, Preprint TM-682 (Batavia: Fermilab, 1976); Preprint TM-684 (Batavia: Fermilab, 1976)
29. Elishev A F et al. *Phys. Lett. B* **88** 387 (1979)
30. Moller S P, in *CERN Accelerator School* (CERN 94-05) (Geneva: CERN, 1994) p. 1
31. Asseev A A et al. *Nucl. Instrum. Meth. Phys. Res. A* **324** 31 (1993)
32. Baldin A M et al. *AIP Conf. Proc.* **2** 131 (1971)
33. Baldin A M, Baldin A A *Phys. Part. Nucl.* **29** 232 (1998); *Fiz. Elem. Chastits At. Yadra* **29** 577 (1998)
34. Stavinskii V S *Fiz. Elem. Chastits At. Yadra* **10** 949 (1979)
35. Bayukov Yu D et al. *Izv. Akad. Nauk SSSR. Ser. Fiz.* **30** 521 (1966)
36. Baldin A M et al., in *Trudy Chetvertogo Vsesoyuz. Soveshch. po Uskoritelyam Zaryazhennykh Chastits, Moskva, 18–20 Noyabrya 1974 g.* (Proc. of the 4th All-Russian Workshop on Charged Particle Accelerators, Moscow, 18–20 November 1974) Vol. 2 (Moscow: Nauka, 1975) p. 4
37. Aksinenko V D et al. *Instrum. Exp. Tech.* **30** 601 (1987); *Prib. Tekh. Eksp.* (3) 97 (1987)
38. Anikina M Kh et al. *Phys. Atom. Nucl.* **72** 439 (2009); *Yad. Fiz.* **72** 473 (2009)
39. Podgoretskii M I *Sov. J. Part. Nucl.* **20** 266 (1989); *Fiz. Elem. Chastits At. Yadra* **20** 628 (1989)
40. Abashidze L I et al. *Instrum. Exp. Tech.* **28** 767 (1985); *Prib. Tekh. Eksp.* (4) 33 (1985)

41. Avdeichikov V V et al. *Sov. J. Nucl. Phys.* **48** 1043 (1988); *Yad. Fiz.* **48** 1736 (1988)
42. Karnaukhov V A et al. *Phys. Atom. Nucl.* **62** 237 (1999); *Yad. Fiz.* **62** 272 (1999)
43. Karnaukhov V A *Phys. Part. Nucl.* **37** 165 (2006); *Fiz. Elem. Chastits At. Yadra* **37** 313 (2006)
44. Karnaukhov V A et al. *Phys. Rev. C* **67** 011601(R) (2003)
45. Randrup J, Cleymans J *Phys. Rev. C* **74** 047901 (2006)
46. Sissakian A N, Sorin A S, Toneev V D, in *Proc. of the 33rd Intern. Conf. on High Energy Physics, ICHEP'06, Moscow, Russia, July 26 – August 2, 2006* Vol. 1 (Eds A Sissakian, G Kozlov, E Kolganova) (New Jersey: World Scientific, 2007) p. 421
47. Trubnikov G et al., in *Particle Accelerator. Proc. of the 11th European Conf., EPAC 2008, Genoa, Italy, June 23 – 27, 2008* (Eds I Andrian, C Petit-Jean-Genaz) (Geneva: CERN, 2008) p. 2581
48. NICA White Paper, http://theor.jinr.ru/twiki-cgi/view/NICA/WebHome
49. Meshkov I N *Phys. Atom. Nucl.* **75** 594 (2012); *Yad. Fiz.* **75** 637 (2012)
50. Kuznetsov A B, Meshkov I N, Philippov A V *Phys. Part. Nucl. Lett.* **9** 346 (2012); *Pis'ma Fiz. Elem. Chastits At. Yadra* **9** 576 (2012)
51. Philippov AV, Kuznetsov A B, Meshkov I N *Phys. Part. Nucl. Lett.* **8** 1087 (2011); *Pis'ma Fiz. Elem. Chastits At. Yadra* **8** (10) 87 (2011)
52. Kekelidze V D et al., in *Proc. of the 36th Intern. Conf. on High Energy Physics, ICHEP2012, Melbourne, Australia, July 4 – 11, 2012* (PoS ICHEP2012) (2013) p. 411
53. Alt C et al. (NA49 Collab.) *Phys. Rev. C* **77** 024903 (2008); arXiv: 0710.0118
54. Krasavin E A *Phys. Usp.* **59** 411 (2016); *Usp. Fiz. Nauk* **186** 435 (2016);
55. Kadykov M G et al. *Phys. Part. Nucl. Lett.* **10** 573 (2013); *Pis'ma Fiz. Elem. Chastits At. Yadra* **10** 936 (2013)
56. Khodzhibagiyan H G et al. *IEEE Trans. Appl. Supercond.* **24** 4001304 (2014)
57. Khodzhibagiyan H G, Kovalenko A D, Fisher E *IEEE Trans. Appl. Supercond.* **14** 1031 (2004)
58. Stassen R et al., in *Beam Cooling and Related Topics. Proc. of the Workshop, COOL 07, Bad Kreuznach, Germany, September 9 – 14, 2007* (Eds R W Hasse, V R W Schaa) (Darmstadt: GSI, 2007) p. 191; http://accelconf.web.cern.ch/AccelConf/cl07/INDEX.HTM
59. Kobets A G et al. *Phys. Part. Nucl. Lett.* **9** 364 (2012); *Pis'ma Fiz. Elem. Chastits At. Yadra* **9** 604 (2012)
60. Ahmanova E V et al., in *Proc. of the Russian Particle Accelerator Conf, RuPAC'2014, Obninsk, Russia, 6 – 10 October 2014* (Obninsk, 2014) p. 85; http://accelconf.web.cern.ch/AccelConf/rupac2014/
61. Parkhomchuk V V, in *Proc. of the Intern. Workshop on Beam Cooling and Related Topics, COOL2013, 10th – 14th June 2013, Mürren, Switzerland* (Eds L V Jørgensen, V R W Schaa) (Geneva: CERN, 2013) p. 55; http://accelconf.web.cern.ch/AccelConf/COOL2013/
62. Shemyakin A V et al., in *Beam Cooling and Related Topics. Proc. of the Workshop, COOL'11, Alushta, Ukraine, September 12 – 16, 2011* (Ed. M V Kuzin) (Dubna: JINR, 2011) p. 5; http://accelconf.web.cern.ch/AccelConf/COOL2011/index.htm
63. Gorbachev E V et al., in *Particle Accelerator. Proc. of the 21st Russian Conf., RuPAC 2008, Zvenigorod, Russia, September 28 – October 3, 2008* (Eds M V Kuzin, E E Shirkova, A V Philippov) (Dubna: JINR, 2008) p. 97; http://accelconf.web.cern.ch/AccelConf/r08/
64. Zhabitsky V M *Phys. Atom. Nucl.* **45** 472 (2014); *Fiz. Elem. Chastits At. Yadra* **45** 806 (2014)
65. Agapov N N *Phys. Part. Nucl.* **30** 322 (1999); *Fiz. Elem. Chastits At. Yadra* **30** 760 (1999)
66. Agapov N N et al., in *Proc. of the 12th Cryogenics 2012 IIR Conf., Dresden, Germany, September 11 – 14, 2012* (Praha: Icaric Ltd, 2012) p. 12